

EP/L014106/1
Supergen Wind Hub
 Sustainable Power Generation and Supply
 - Wind Energy Technologies



Deliverable 5.1.2

Report on assessment of Stress concentration method for innovative blade design

Delivered by:	¹ STFC Rutherford Appleton Laboratory		
Author(s):	Blanca Pascual ¹		
Delivery date:	31 st May 2017		
Distribution list:	Supergen Wind Consortium		
Version No	Status	Date	Checked by
1	Draft	31 st May 2017	T.Davenne and J.Halliday

Sponsored by



1 Introduction

The UK has a target of over 30% energy from renewables by 2020 to reduce its CO₂ emissions. For this, onshore and offshore wind have to increase their capacity, from 10.1GW and 5.3GW in May 2017, respectively to 13GW and 18GW by 2020. The SUPERGEN Wind Energy Technologies Consortium is a UK wind energy research consortium which was originally established by the EPSRC on 23rd March 2006 as part of its Sustainable Power Generation and Supply (SUPERGEN) programme. Its aim is to develop academic, industrial and policy linkages and to lead the technology strategy for driving forward UK wind energy research and for exploiting the research outcomes. This in turn should address the medium term challenges of scaling up to multiple wind farms, considering how to better build, operate and maintain multi-GW arrays of wind turbines whilst providing a reliable source of electricity whose characteristics can be effectively integrated into a modern power system such as that in the UK. The consortium is led by Strathclyde University, but also includes Durham, Loughborough, Cranfield, Manchester, Oxford, Surrey, Bristol, Imperial, Dundee and STFC, with expertise in wind turbine technology, aerodynamics, hydrodynamics, materials, electrical machinery, control, reliability and condition monitoring, and has the support of 18 industrial partners, including DNV GL and the Offshore Renewable Energy Catapult. Its activities were renewed in 2014, and is funded to 2019.

This report is related to work package 5.1, on innovative blade design for improved load control, where the use of sub-modelling is explored in ABAQUS to determine the extent to which this might improve the modelling and representation of the structural loads without adding unduly to processing time.

This report studies the use of sub-modelling in ABAQUS to improve the representation of stresses without adding unduly to the processing time.

The operating lifetime of wind turbine blades is controlled by the fatigue properties of the composite materials they're made of. These materials are generally provided as fabrics (non-crimp fabrics, uniweave, woven), i.e. they have a 2D nature that is reconfigured into 3D shapes when the blade and its internal features (e.g. spars) are formed. Methods to assess fatigue life damage for 2D composites with in-plane loading have been the subject of several studies [3] but in regions such as the T-joint joining the blade spar to the aerodynamic profile, through thickness effects are non-negligible and 3D stress states have to be taken into account.

The initiation of damage in these regions can occur well before what would be expected in the base material subjected to in-plane loading. Numerical studies of these geometry-related fatigue issues are generally performed on test models of dimensions in the order of 0.1m [4, 5, 7], using a very fine solid elements mesh. Wind turbine blade FE models available for academic purposes have lengths two to three orders of magnitude larger than these T-joint test samples: e.g. the DTU 10MW turbine is 86.5m long [1]. These blade FE models use shell elements. Embedding the T-joint fine solid mesh within the shell mesh, so as to obtain an accurate stress assessment, could be both computationally challenging and need a detailed knowledge of the geometry.

Here, the method proposed in the previous report [6] is further explored to use different test cases and vectors for the decomposition.

2 Validation models loading and geometry

2.1 Blade element momentum loads

In the previous report [6], a long extruded profile blade model was constructed using the ideal aerodynamic section forces from blade element momentum (BEM), and these forces were

applied as pressures. Gravity and centrifugal forces were also applied. The section forces from BEM are [2]

$$\mathbf{F}_y = 2\rho a(1-a)v_0^2 A/3 \quad \mathbf{F}_x = 2\rho(1-a)v_0 A \Omega a' R/3 \quad a = 1/3 \quad a' = \frac{a(1-a)}{\lambda R/R_{max}} \quad (1)$$

with $\rho = 1.225 \text{ kg/m}^3$ the air density, v_0 the wind speed, A the area of an annular ring of the actuator disc considered ($A = \pi(R_e^2 - R_i^2)$), a the axial flow induction factor that maximizes the power coefficient when the turbine is modelled as an actuator disc (e.g. [2]), a' is the tangential flow induction factor, Ω is the angular velocity, R the radius of the ring considered, R_{max} is the total radius of the rotor, $\lambda = \Omega * R_{max}/v_0$ is the tip speed ratio. The blade is also subjected to centrifugal load ($\Omega = 2.8 \text{ rad/s}$) and gravity load, with the gravity pointing in the $-z$ direction, the root of the blade located at $Z=0$, and the tip at $Z=-25\text{m}$.

2.2 Blade model geometries used for validation

Two simplified blade models are used to validate results, the extruded profile used for the test cases, and a blade using the same profile but following a given chord and twist distribution along the length of the blade. This second blade was constructed because the geometry of the test cases and of the long extruded profile blade used in the previous report [6] is the same, and the method should be tested with a different geometry to assess both that it can be used with a different geometry and that it is suitable for blades with changes in twist and chord.

2.2.1 Long Extruded profile

The geometry of this model is the one used to benchmark the results of the test cases in the previous report [6]. In that report [6], the comparison results were not acceptable, as the stresses from the loaded blade and from the proposed method were very different. Here, it has been decided to use the same geometry for the test cases described in subsection 3.1 and for the first validation model. The loading in this validation model attempts to simulate a rotation of the blade. This load includes a gravity load that changes its angle, so as to simulate the rotation, a centrifugal load, and a pressure distribution displayed in Figure 1b equivalent to the BEM loading. The test cases and the validation model are studied in different steps of the same analysis, as they both use the same mesh, so that the test cases are computed in steps 1 to 12 and the rotation is studied in the last step. The model includes three kinematic couplings, displayed in figure 2. For all the steps (test cases and rotation), the control node of the kinematic coupling at the root (see Figure 2a) has been fixed. For the test cases, different pressures and displacements are applied in each test case, and these different displacements are applied to the control nodes of the other kinematic couplings included in the model. These other kinematic couplings are located at the tip of the model (Figure 2b) and at an intermediate ring of nodes (Figure 2c). In kinematic couplings, the nodes are slave to the translations and rotations of the control node of the coupling. The elements where pressures are applied are highlighted in Figures 2d and 2e.

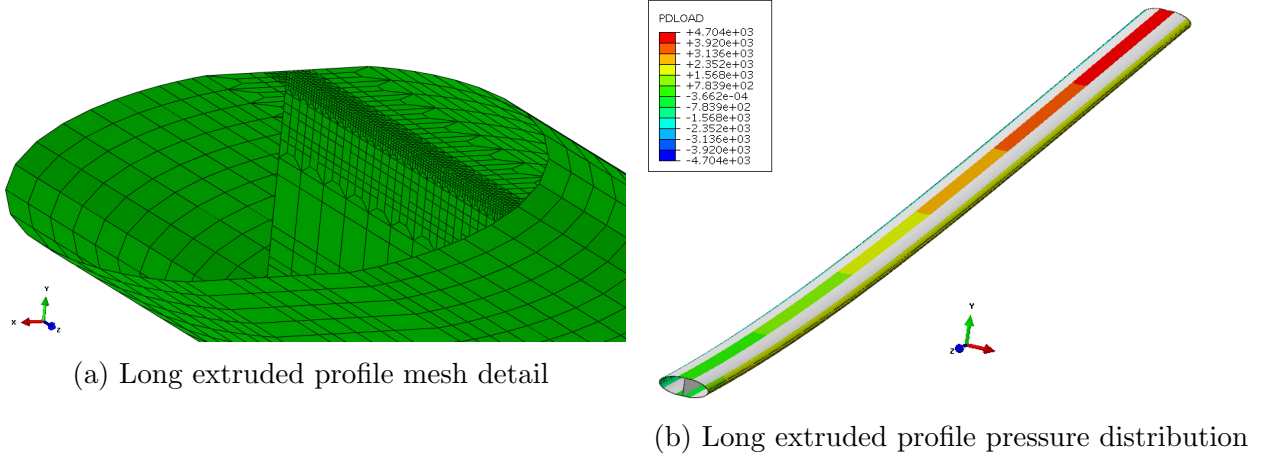


Figure 1: Long extruded profile geometry

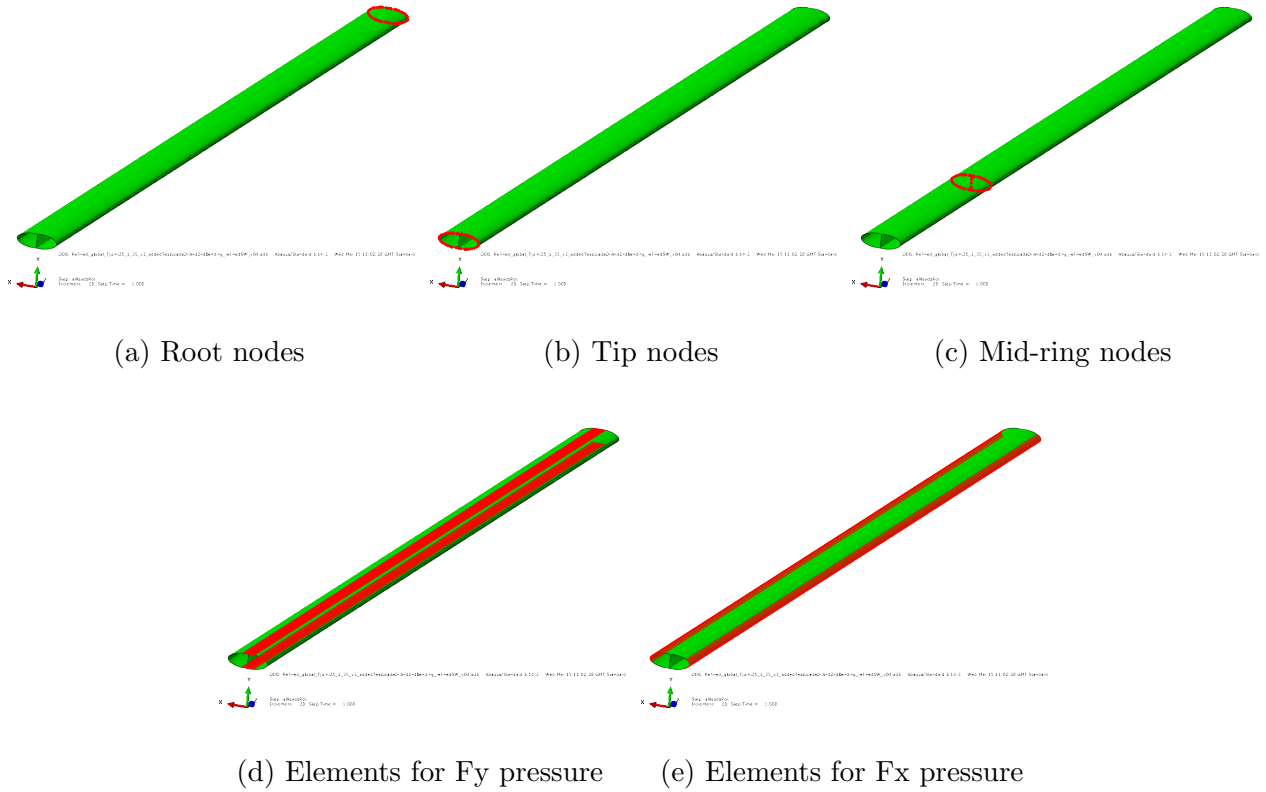


Figure 2: Nodes and elements where BCs/loads are applied to the extruded profile blade model

2.2.2 Profile following chord/twist distribution

This geometry uses the same profile, but it is scaled to modify the chord, and twisted along the length of the blade. The wind energy handbook [2] provides a simplified blade geometry using profile NACA 4412, provided that the drag of the profile is ignored, ideal distributions of a and a' are used, the lift coefficient maximizes lift/drag ratio C_l/C_d at $\mu = 0.7$ and $\mu = 0.9$ span points, and assuming that the chord c_u is linear with the length (straight line drawn through the 0.7 and 0.9 span points) of the blade. Then the chord, using a constant value of $C_l = 0.7$, is given by

$$\frac{c_u}{R_{max}} = \frac{8}{9\lambda 0.8} \left(2 - \frac{\mu}{0.8} \right) \frac{2\pi}{C_l \lambda N} \quad (2)$$

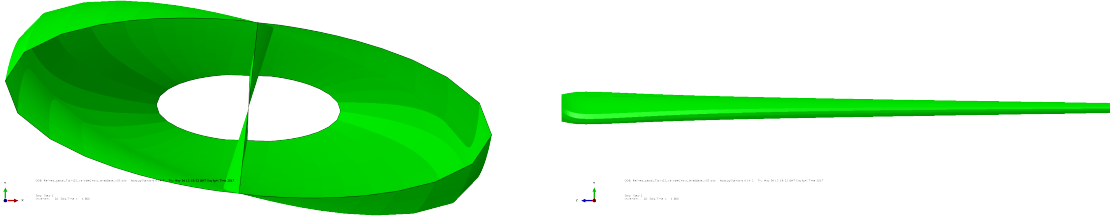
with $\mu = R/R_{max}$, N the number of blades (here we assume three blades) and we assume the aerodynamic properties are as in NACA 4412, i.e. $C_l = 0.7$ for an angle of attack $\alpha = C_l/0.1 - 4$ (in degrees), that is constant along the blade length. The distribution of the lift coefficient can then be obtained from the chord distribution

$$C_l = \frac{8}{9} \frac{1}{\frac{Nc_u\lambda}{2\pi} \sqrt{(2/3)^2 + \lambda^2\mu^2} \left[1 + \frac{2}{9\lambda^2\mu^2}\right]^2} \quad \alpha = C_l/0.1 - 4 \quad (3)$$

and α is the angle of attack. The local inflow angle ϕ at each blade station varies along the blade is

$$\tan \phi = \frac{1 - a}{\lambda\mu(1 + a')} = \frac{1 - 1/3}{\lambda\mu \left(1 + \frac{2}{9\lambda^2\mu^2}\right)} \quad \beta = \phi - \alpha \quad (4)$$

So that the β is the twist of the blade. Here, the profile used is the one described in section 2.2.1 instead of NACA 4412, but the chord and twist distribution provided in Equations 2 and 4 are used. The pressures applied on the leading edge/trailing edge surfaces (P_{LE-TE}) and top and bottom surfaces (P_{T-B}), lead to the same aerodynamic forces as the ones obtained from BEM in equation 1. The new pressures are now applied on surfaces that have been twisted by an angle β , and, for the leading and trailing edge surfaces, these surfaces have also been scaled with the chord, and are equivalent to forces F'_y aligned with the LE-TE axis, and F'_x , perpendicular to this one. These forces can be related to F_y and F_x in equation 1 through $F'_x = \cos\beta F_x - \sin\beta F_y$, $F'_y = \sin\beta F_x + \cos\beta F_y$



(a) Twist of the blade, seen from the root

(b) Chord of the blade

Figure 3: Twist and chord of the blade

3 Method and test cases

The method was described in the previous report [6], and consists in the following steps

1. Create test cases using shell elements, all using the same geometry but different loads. The test cases used are further explained in subsection 3.1.
2. Extract vectors of data \mathbf{v} for each of the test cases. Different vectors can be used with this method, the ones perused here are described in subsection 3.2.
3. Create solids submodels for the T-joint region of the test cases, so as to have a detailed representation of the stresses at the T-joint for the test cases.
4. Create a matrix whose columns are the data vectors from the test cases obtained in step 2, i.e. $\mathbf{V} = [\mathbf{v}_1, \dots, \mathbf{v}_i]$. Calculate its Moore-Penrose pseudo-inverse \mathbf{V}_{MP}^{-1}
5. From the blade shell model subjected to aerodynamic, centrifugal, gravity, gyroscopic loading: obtain a vector of data \mathbf{v}_g , similar to the one from the test cases in step 2.

6. Pre-multiply the vector from Step 5 by the Moore-Penrose pseudo-inverse of Step 4. This results in a vector of coefficients $\alpha = \mathbf{V}_{MP}^{-1} \mathbf{v}_g$.
7. Combine the test cases submodels using the vector of coefficients α from Step 6. This results in detailed stresses around the T-joint.

3.1 Long extruded profile test models

The geometry and couplings of this test model have been described in subsection 2.2.1. For the test cases, data is extracted to form the vectors in Step 2 at the integration point of elements highlighted in Figure 4. These elements are of size $t \times t$ (where t is the thickness of the shell), so that data at distances $0.5t$, $1.5t$ and $2.5t$ from the T-joint can be extracted easily

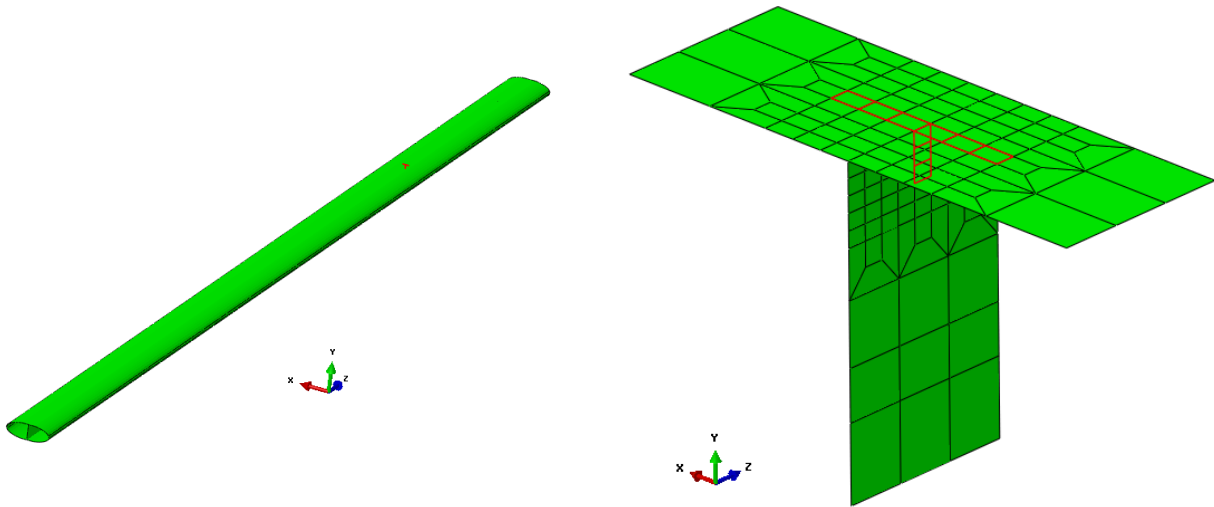


Figure 4: Elements where stresses and strains are extracted

The test cases used with this geometry all have the control node of the kinematic coupling linking nodes at the root (Figure 2a) fixed in all its degrees of freedom. The other loading and BCs applied in each test case are

1. Gravity in Z direction: a distributed gravity load in the -Z direction is applied to all elements.
2. Gravity in X direction: a distributed gravity load in the X direction is applied to all elements.
3. Gravity in Y direction: a distributed gravity load in the Y direction is applied to all elements.
4. Centrifugal load: assumes the rotation speed is 2.8rad/s (tip speed ratio of 7, wind speed of 10m/s)
5. Pull-out: applies a pressure of 10Pa on the elements in Figure 2d
6. Pinch sides: Applies a pressure of 10Pa on the elements in Figure 2e
7. Tip z displacement: the control node of the kinematic coupling at the tip, controlling nodes in Figure 2b is displaced 0.1m in the Z direction.

8. Tip x displacement: the control node of the kinematic coupling at the tip is displaced 0.1m in the X direction.
9. Tip y displacement: the control node of the kinematic coupling at the tip is displaced 0.1m in the Y direction.
10. Tip Rz rotation: the control node of the kinematic coupling at the tip, is rotated 0.1rad in the Y direction.
11. Mid ring x displacement: the control node of the kinematic coupling controlling nodes from Figure 2c is displaced 0.1m in the X direction.
12. Mid ring y displacement: the control node of the kinematic coupling controlling nodes from Figure 2c is displaced 0.1m in the Y direction.

The displacements of the above test functions are given in figure 5

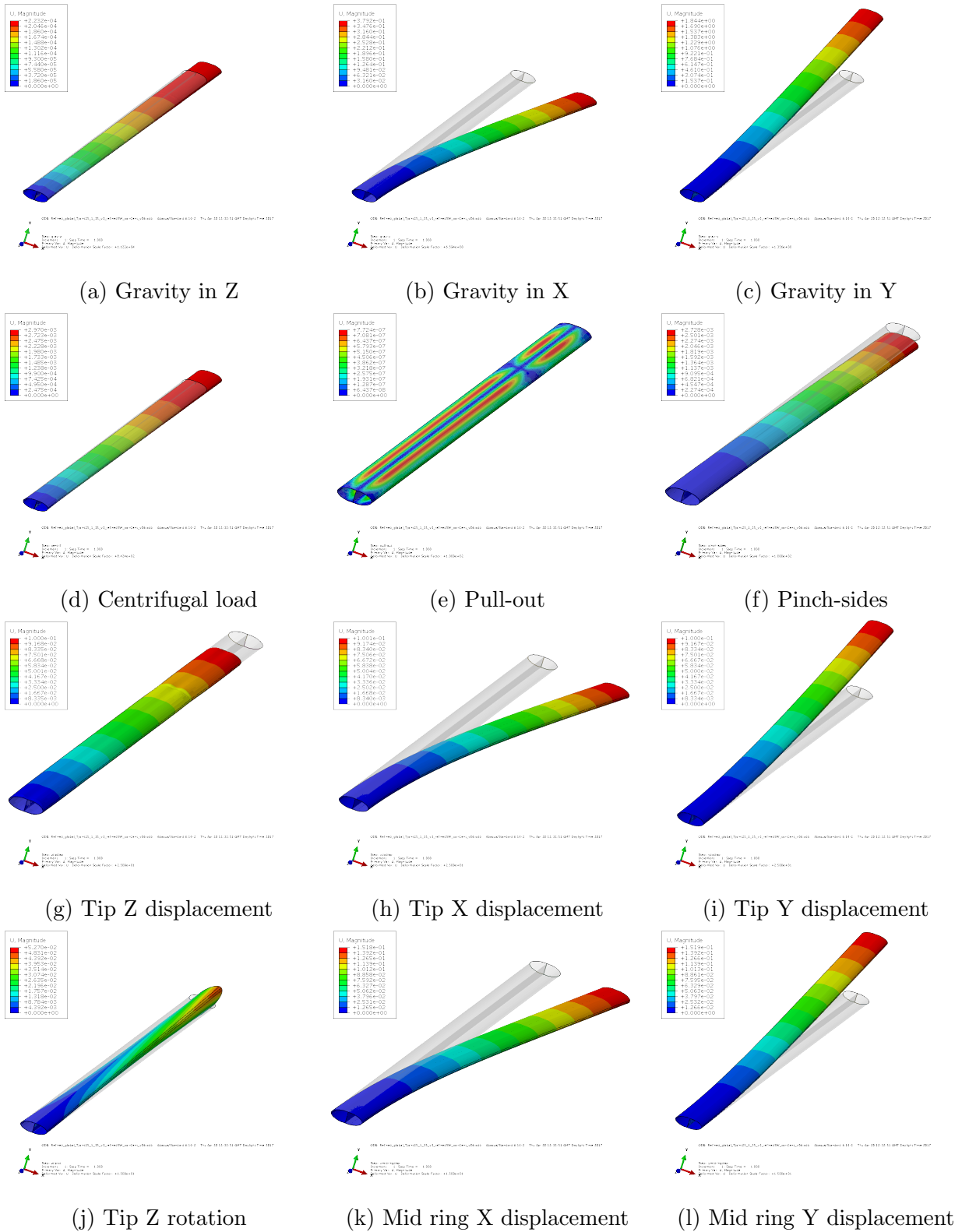


Figure 5: Extruded profile test cases displacement

3.2 Vectors of the subspace used in the proposed decomposition method

In the previous report [6], six types of vector were proposed as bases of six corresponding subspaces. Some of these vectors are no longer reported, and some new vectors are described, namely Vector 3 and Vector 5. The results reported in section 4 will calculate the different α

vectors based on the bases obtained from

Vector 1 Corresponds to the first vector discussed in the previous report [6]. Vector obtained from shell element membrane strains and curvatures in local 1 and 2 axis (outputs ‘SE1’, ‘SE2’, ‘SE3’, ‘SK1’, ‘SK2’, in abaqus) are extracted at 0.5t and 1.5t, i.e. for an element on the outer skin and right side of the shear web, and at a distance 1.5t of the T-joint, a vector $\mathbf{v}'_{OSR,1.5} = [SE1, SE2, SE3, SK1, SK2]$ is created. This leads to 5 (strains/curvatures) x 2 (distances from T-joint) x 3 (sides around the T-joint: outer skin right, outer skin left and shear web) = 30 datum to be used in each data vector of the test cases/global model, so that the data vector is given by

$$\mathbf{v} = \begin{bmatrix} \mathbf{v}_{OSR,0.5} \\ \mathbf{v}_{OSR,1.5} \\ \mathbf{v}_{OSL,0.5} \\ \mathbf{v}_{OSL,1.5} \\ \mathbf{v}_{SW,0.5} \\ \mathbf{v}_{SW,1.5} \end{bmatrix} \quad \text{with} \quad \mathbf{v}_{OSR,0.5} = \begin{bmatrix} SE1_{OSR,0.5} \\ SE2_{OSR,0.5} \\ SE3_{OSR,0.5} \\ SK1_{OSR,0.5} \\ SK2_{OSR,0.5} \end{bmatrix} \quad (5)$$

It is noted that results obtained with this basis are only displayed for the straight blade at location 1 in Figure 8, where this method performs poorly in comparison with the other ones.

Vector 2 Corresponds to the fourth vector discussed in the previous report [6]. Vector obtained from shell membrane strains at the top and bottom of the shells (‘E11’, ‘E22’ and ‘E12’ outputs in abaqus for the topmost and bottommost section points of the shells) at distances 0.5t and 1.5t of the T-joint. This leads to 3 (strains) x 2 (top/bottom shell location) x 2 (distances from T-joint) x 3 (shells around the T-joint) = 36 datum to be used in each data vector of the test cases/global model.

$$\mathbf{v} = \begin{bmatrix} \mathbf{v}_{OSR,top} \\ \mathbf{v}_{OSR,bottom} \\ \mathbf{v}_{OSL,top} \\ \mathbf{v}_{OSR,bottom} \\ \mathbf{v}_{SW,top} \\ \mathbf{v}_{SW,bottom} \end{bmatrix} \quad \text{with} \quad \mathbf{v}_{OSR,top} = \begin{bmatrix} E11_{OSR,top,0.5t} \\ E22_{OSR,top,0.5t} \\ E12_{OSR,top,0.5t} \\ E11_{OSR,top,1.5t} \\ E22_{OSR,top,1.5t} \\ E12_{OSR,top,1.5t} \end{bmatrix} \quad (6)$$

Vector 3 New vector introduced in this report. Vector obtained from shell membrane strains at the top and bottom of the shells at distances 1.5t and 2.5t from the T-joint. The data vector has a size of 3x2x2x3=36

$$\mathbf{v} = \begin{bmatrix} \mathbf{v}_{OSR,top} \\ \mathbf{v}_{OSR,bottom} \\ \mathbf{v}_{OSL,top} \\ \mathbf{v}_{OSR,bottom} \\ \mathbf{v}_{SW,top} \\ \mathbf{v}_{SW,bottom} \end{bmatrix} \quad \text{with} \quad \mathbf{v}_{OSR,top} = \begin{bmatrix} E11_{OSR,top,1.5t} \\ E22_{OSR,top,1.5t} \\ E12_{OSR,top,1.5t} \\ E11_{OSR,top,2.5t} \\ E22_{OSR,top,2.5t} \\ E12_{OSR,top,2.5t} \end{bmatrix} \quad (7)$$

Vector 4 Corresponds to the sixth vector discussed in the previous report [6]. Vector obtained from shell membrane strains at the top and bottom of the shells at distances 0.5t,

1.5t and 2.5t from the T-joint. The data vector has a size of $3 \times 2 \times 3 \times 3 = 54$

$$\mathbf{v} = \begin{bmatrix} \mathbf{v}_{OSR,top} \\ \mathbf{v}_{OSR,bottom} \\ \mathbf{v}_{OSL,top} \\ \mathbf{v}_{OSR,bottom} \\ \mathbf{v}_{SW,top} \\ \mathbf{v}_{SW,bottom} \end{bmatrix} \quad \text{with} \quad \mathbf{v}_{OSR,top} = \begin{bmatrix} E11_{OSR,top,0.5t} \\ E22_{OSR,top,0.5t} \\ E12_{OSR,top,0.5t} \\ E11_{OSR,top,1.5t} \\ E22_{OSR,top,1.5t} \\ E12_{OSR,top,1.5t} \\ E11_{OSR,top,2.5t} \\ E22_{OSR,top,2.5t} \\ E12_{OSR,top,2.5t} \end{bmatrix} \quad (8)$$

Vector 5 New vector introduced in this report. This vector tries to establish if adding stresses to the vector of data improves the accuracy of the method. Vector obtained from shell membrane strains and shell stresses at the top and bottom of the shells ('E11', 'E22', 'E12', 'S11', 'S22' and 'S12' outputs in abaqus for the topmost and bottommost section points of the shells) at distances 0.5t and 1.5t of the T-joint. This leads to 6 (strains and stresses) x2 (top/bottom shell location) x 2 (distances from T-joint) x3 (shells around the T-joint) =72 datum to be used in each data vector of the test cases/global model.

$$\mathbf{v} = \begin{bmatrix} \mathbf{v}_{OSR,top} \\ \mathbf{v}_{OSR,bottom} \\ \mathbf{v}_{OSL,top} \\ \mathbf{v}_{OSR,bottom} \\ \mathbf{v}_{SW,top} \\ \mathbf{v}_{SW,bottom} \end{bmatrix} \quad \text{with} \quad \mathbf{v}_{OSR,top} = \begin{bmatrix} E11_{OSR,top,0.5t} \\ E22_{OSR,top,0.5t} \\ E12_{OSR,top,0.5t} \\ E11_{OSR,top,1.5t} \\ E22_{OSR,top,1.5t} \\ E12_{OSR,top,1.5t} \\ S11_{OSR,top,0.5t} \\ S22_{OSR,top,0.5t} \\ S12_{OSR,top,0.5t} \\ S11_{OSR,top,1.5t} \\ S22_{OSR,top,1.5t} \\ S12_{OSR,top,1.5t} \end{bmatrix} \quad (9)$$

3.3 Submodels

The T-joint geometry used here is the same as the one used in [7, 5], and its geometry and layup are described in Figure 6. The orientation is such that the second axis corresponds to the direction of the fibre. The material properties of the uniaxial composite are: elastic moduli $E1 = E3 = 9$ GPa, $E2 = 38$ GPa; Poisson's ratios $\nu_{13} = \nu_{23} = 0.3$, $\nu_{12} = 0.071$; and the shear moduli $G_{12} = G_{23} = 3.6$ GPa, $G_{13} = 3.46$ GPa. Due to the elements orientation, stresses S11 are perpendicular to the fibre, S22 are in the direction of the fibre and S12 are shear stresses.

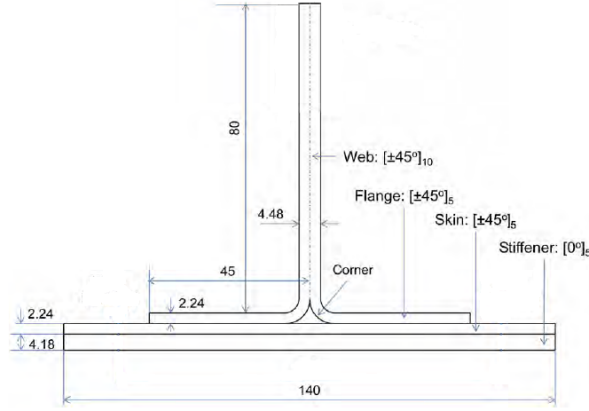


Figure 6: T-joint geometry

The submodels for the test case and the long extruded profile blade have the same geometry. For the blade with twist/chord variation, the T-joint submodel nodes had a change of coordinates, so that for each Z coordinate, all the nodes had their x and y coordinates translated to follow the twist description. This maintains the thickness of the layers, the local radius of the T-joint, the mesh size, and allows to follow the geometry of the blade. Figure 7 provides the mesh for the submodel of the extruded profile blade, and the elements where stresses have been extracted for each ply so as to obtain results in section 4. For all the plies in the shear web, the distance across the radius of the bend is scaled so that they have the same total distance, and the distances in Figure 7 are the ones used as X coordinate in the figures of section 4.

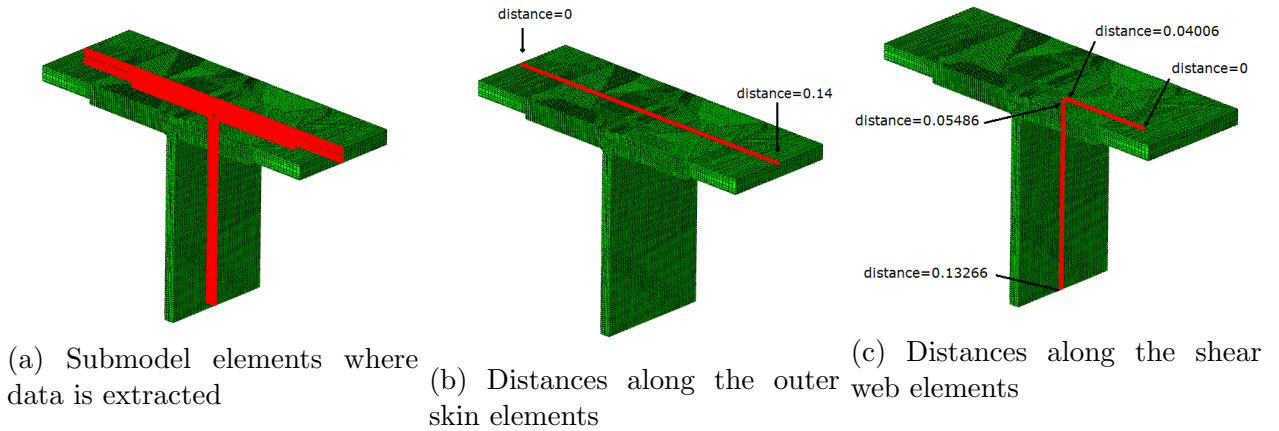


Figure 7: Submodel elements where stresses are extracted, and distances used to plot the results

4 Results

Initially, to check that the method works, a model using the extruded profile geometry was created, where the first step applies gravity in the $-Z$ direction, the second step applies gravity in the X direction, and the third step applies -11 times the gravity in Z direction and -4 times the gravity in the X direction. The coefficients $\alpha_1 = -11$, $\alpha_2 = -4$ were retrieved accurately using the method with the first two steps used as the only two test cases.

Four sets of results are given. Firstly, submodel results are compared for the model with same geometry as the test cases at the same location where the data is extracted (at $Z=-6.18\text{m}$), displayed in black in Figure 8. Then, results are compared at a different Z coordinate within

the T-joint ($Z=-12.38\text{m}$), displayed in red in Figure 8. Then, at the first Z coordinate on the twisted blade from subsection 2.2.2, and finally at the second Z coordinate on the twisted blade.

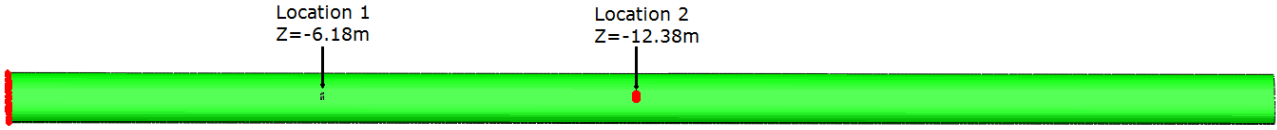
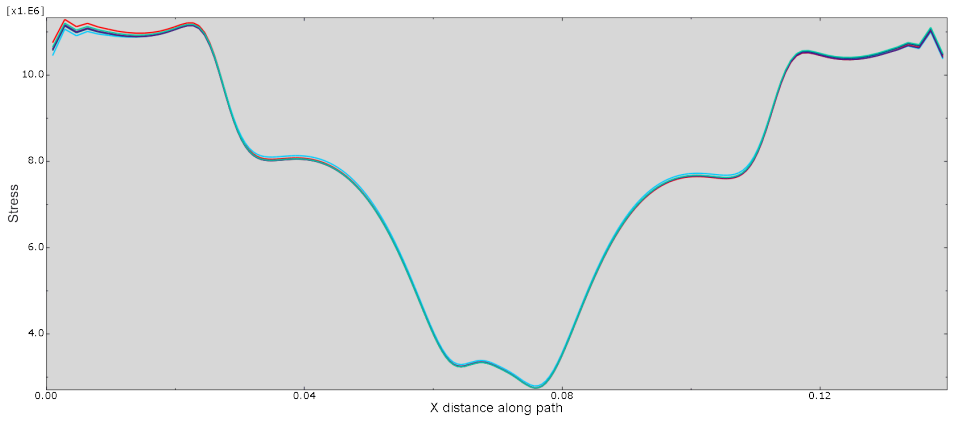


Figure 8: Locations of the submodels in the straight blade (Location 1 in black, location 2 in red)

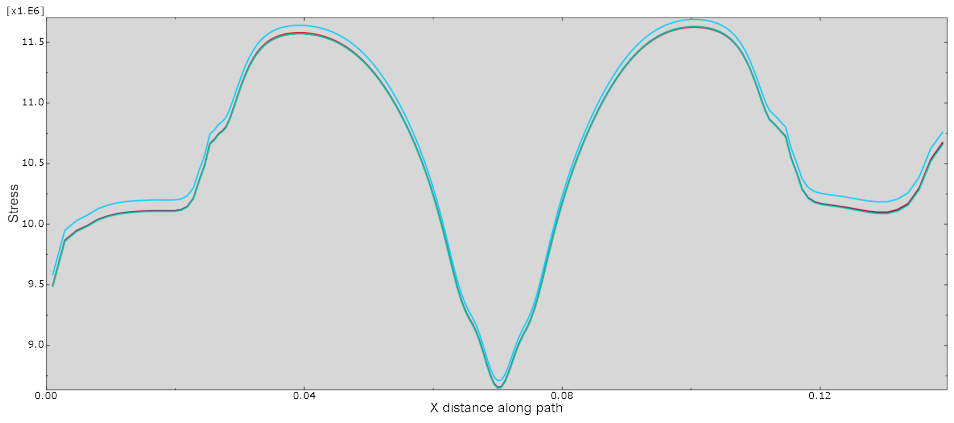
4.1 Results from extruded profile blade at same location

The extruded profile is used for both the test cases and the validation of the results, and data is extracted in both cases at $Z=-6.18\text{m}$. In the last step of the analysis, the blade starts the analysis at the bottom of the rotation, and the rotation is divided into 20 frames, where the analysis is static and the only change between the different frames is the angle of the gravity vector. Results from the 7th frame of the analysis are used for the comparison of stresses obtained directly from the rotating blade submodel and from the method proposed in section 3.

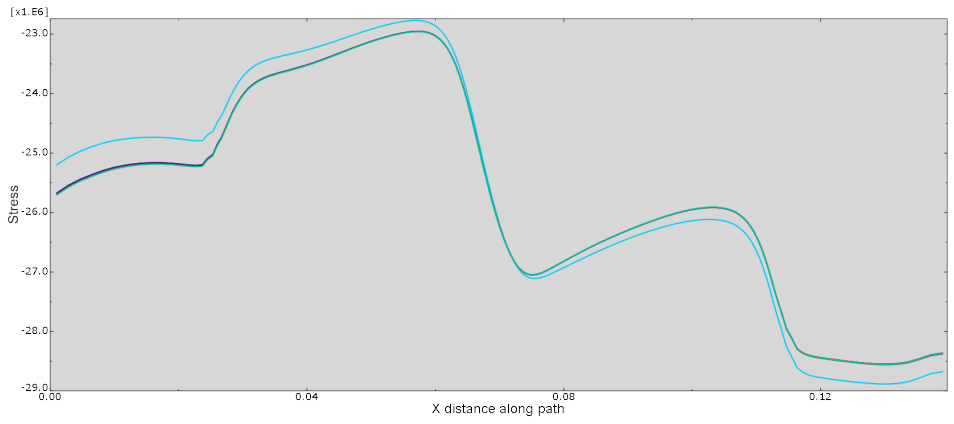
Some examples of the comparison between the stresses on the submodels are given in figures 9, 10, 11, 12, 13 and 14. The red line in each figure provides the results of the submodel of the blade model subjected to distributing loading (BEM, gravity, centrifugal). The remaining lines combine the results of the submodels from the test cases, and differ in the basis of the subspace used to obtain the α coefficients. The cyan, orange, navy and purple lines use, respectively, the shell strains at distances $0.5t$ and $1.5t$ (Vector 1); the strains at top and bottom of the shells at distances $0.5t$ and $1.5t$ (Vector 2); the strains at top and bottom of the shells at distances $0.5t$, $1.5t$ and $2.5t$ (Vector 4); the strains at top and bottom of the shells at distances $1.5t$ and $2.5t$ (Vector 3); The turquoise line uses strains and stresses at top and bottom of the shells at distances $0.5t$ and $1.5t$ (Vector 5)



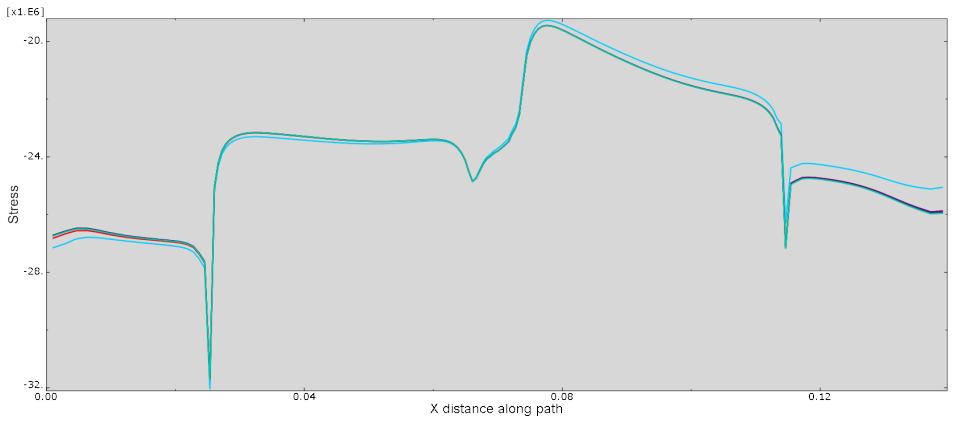
(a) Bottom of ply-1



(b) Middle of ply-5

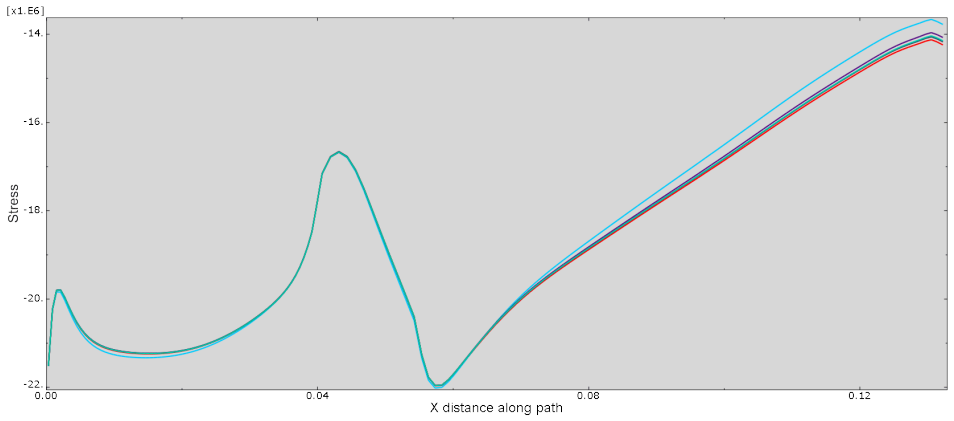


(c) Middle of ply-6

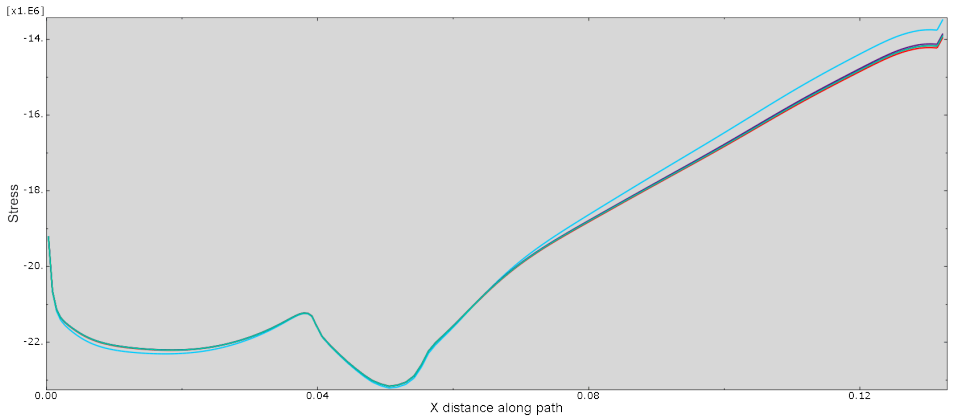


(d) Top of ply 15

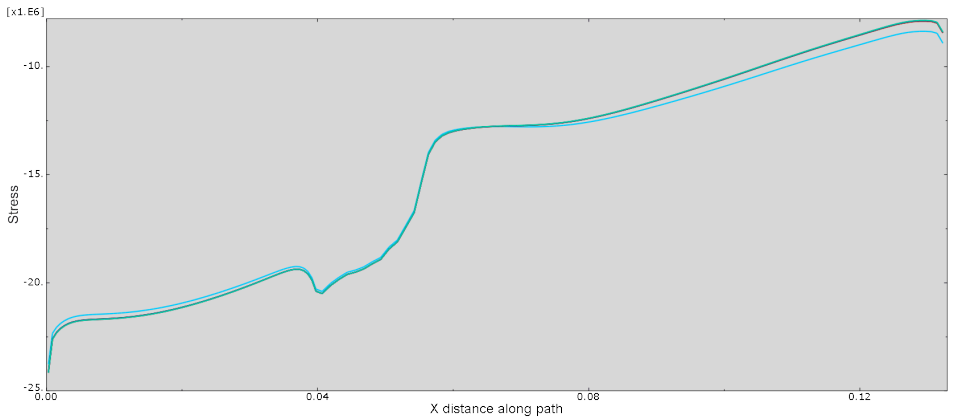
Figure 9: S11 submodel stresses at different plies of the outer skin. The ply is indicated in the caption of each subfigure. Stresses are in Pa, distances in m.



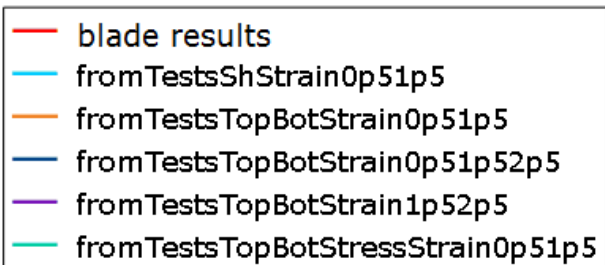
(a) Bottom of ply-1



(b) Top of ply 5

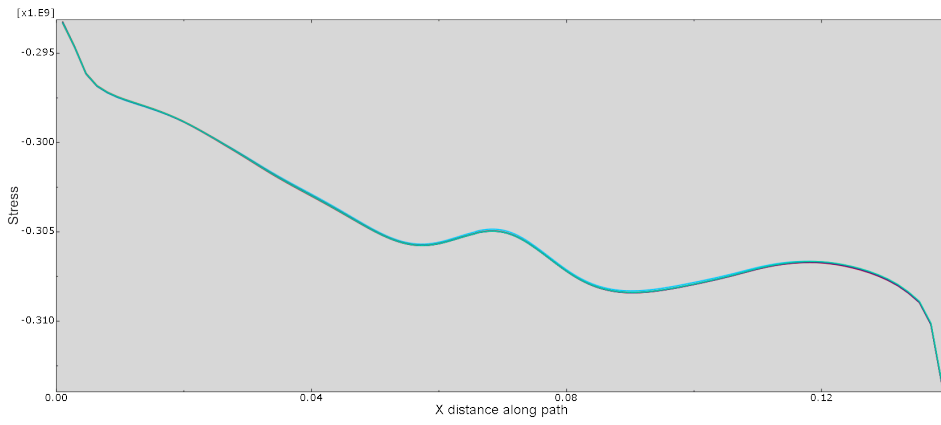


(c) Top of ply 10

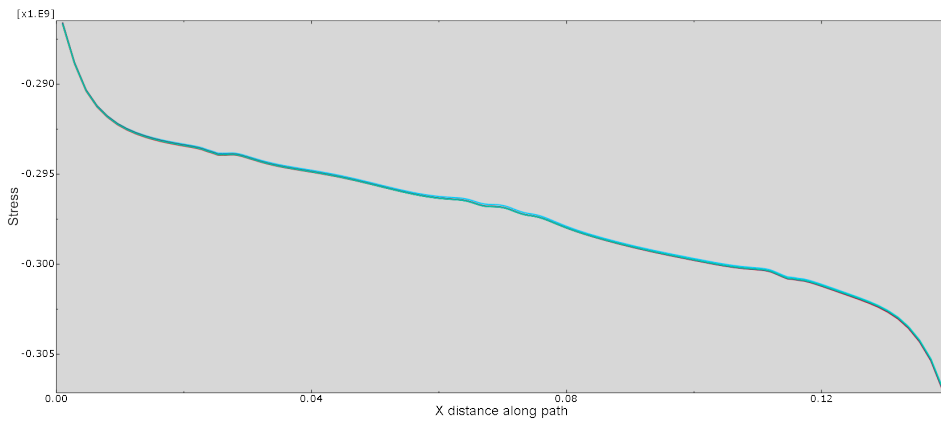


(d) legend

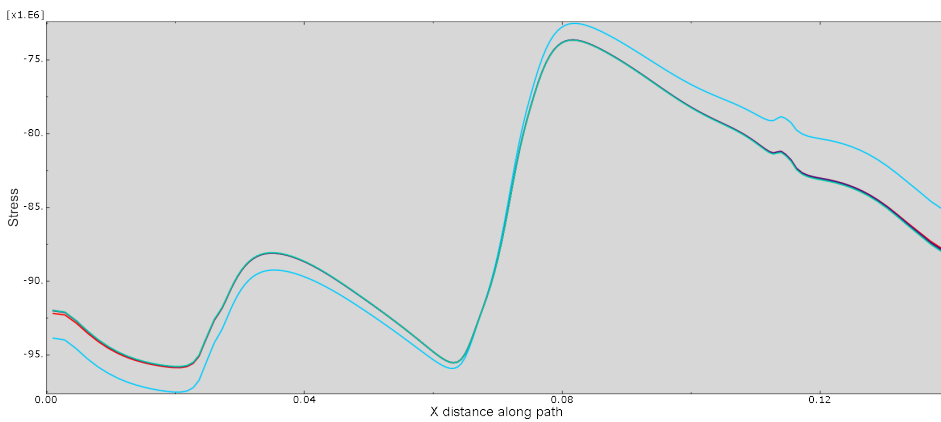
Figure 10: S11 submodel stresses at different plies of the shear web. The ply is indicated in the caption of each subfigure. Stresses are in Pa, distances in m.



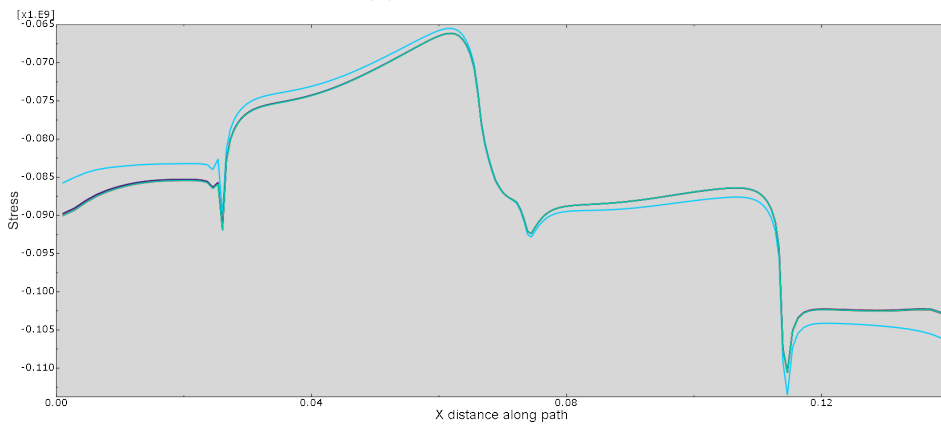
(a) Bottom of ply 1



(b) Middle of ply 5

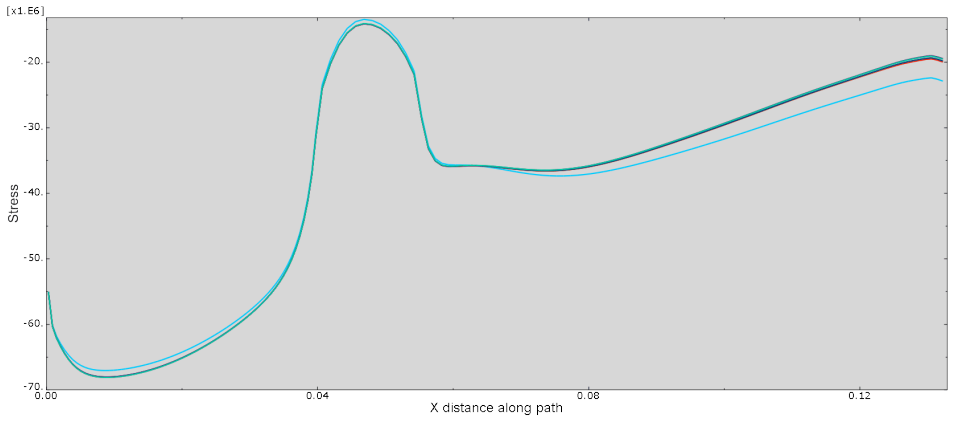


(c) Middle of ply 6

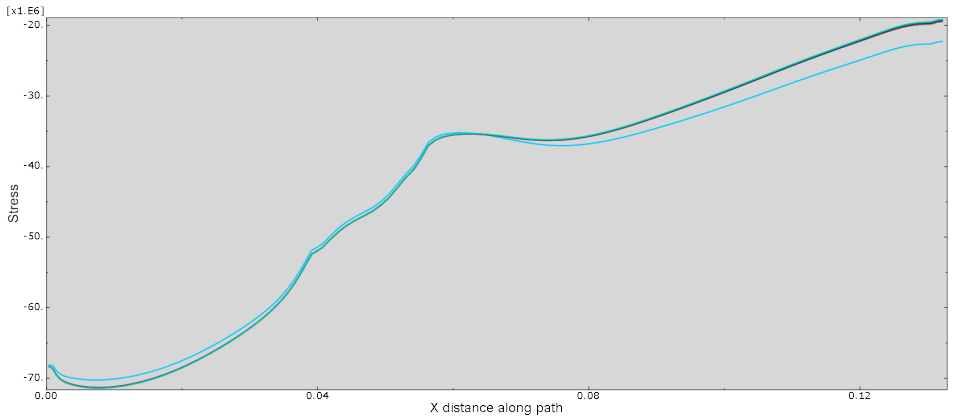


(d) Top of ply 15

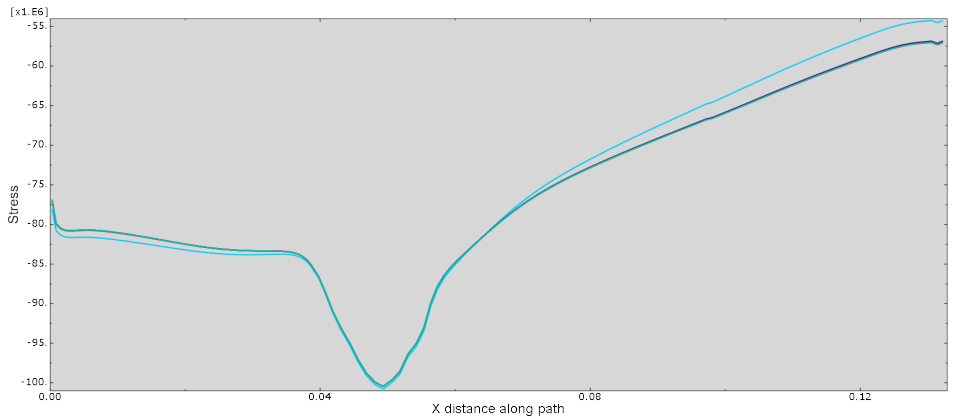
Figure 11: S22 submodel stresses at different plies of the outer skin. The ply is indicated in the caption of each subfigure. Stresses are in Pa, distances in m.



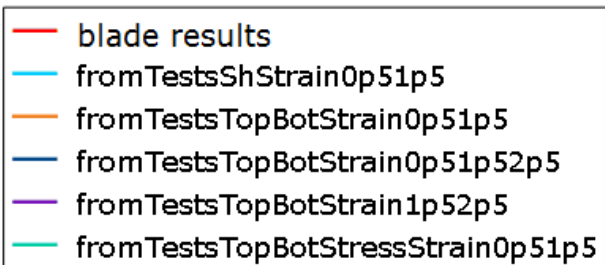
(a) Bottom of ply 1



(b) Top of ply 5

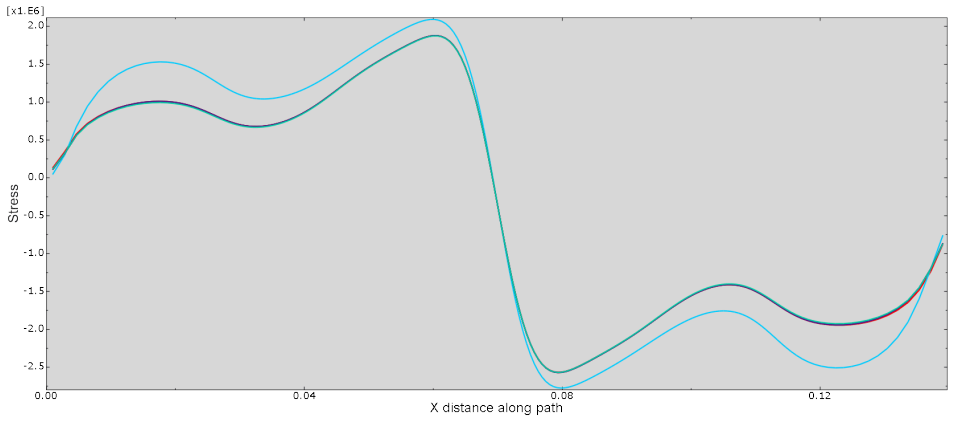


(c) Top of ply 10

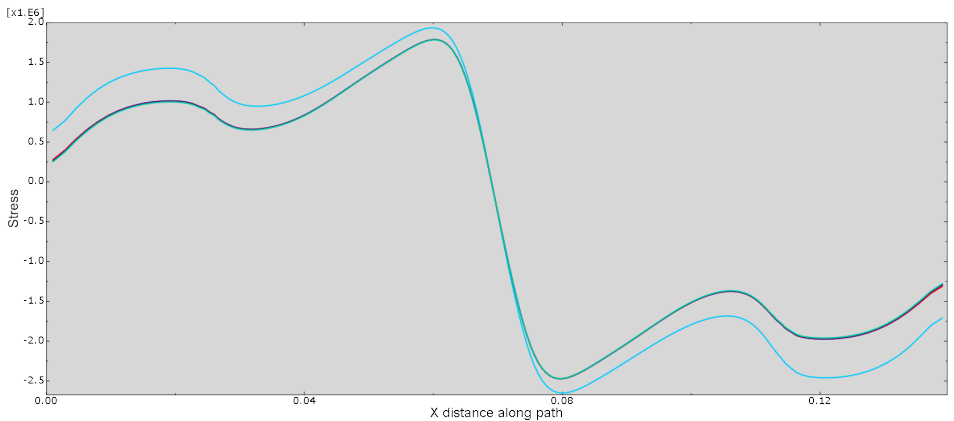


(d) legend

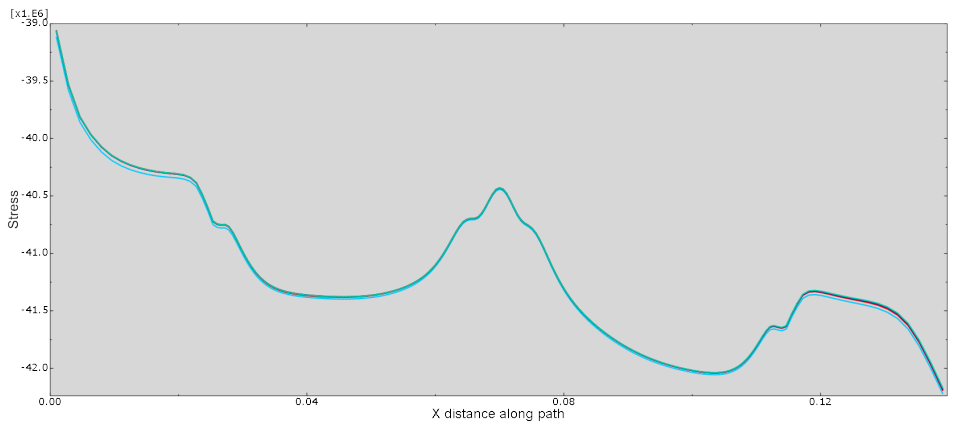
Figure 12: S22 submodel stresses at different plies of the shear web. The ply is indicated in the caption of each subfigure. Stresses are in Pa, distances in m.



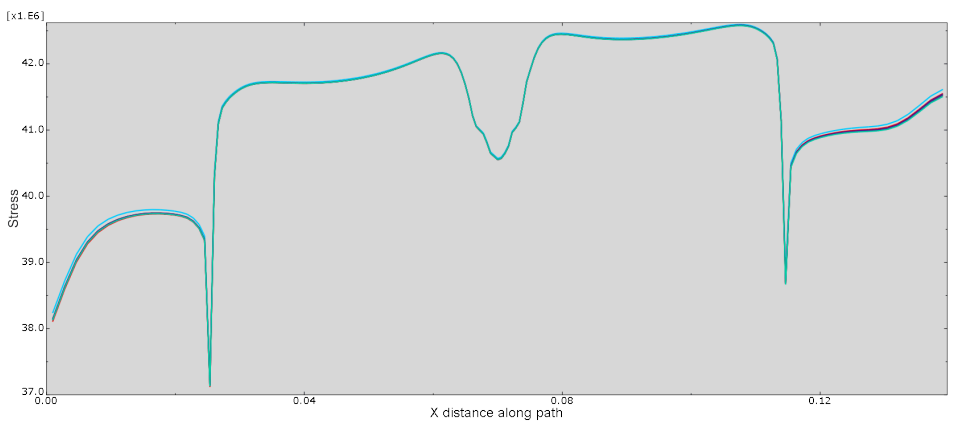
(a) Bottom of ply-1



(b) Middle of ply-5

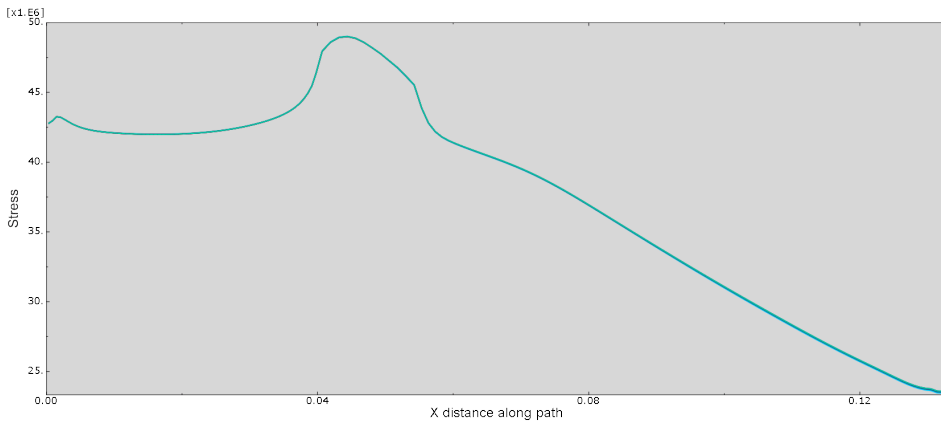


(c) Middle of ply-6

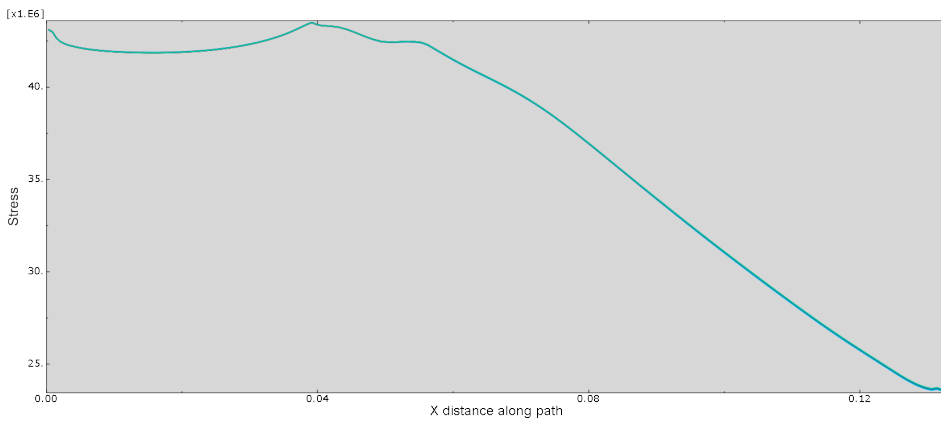


(d) Top of ply-15

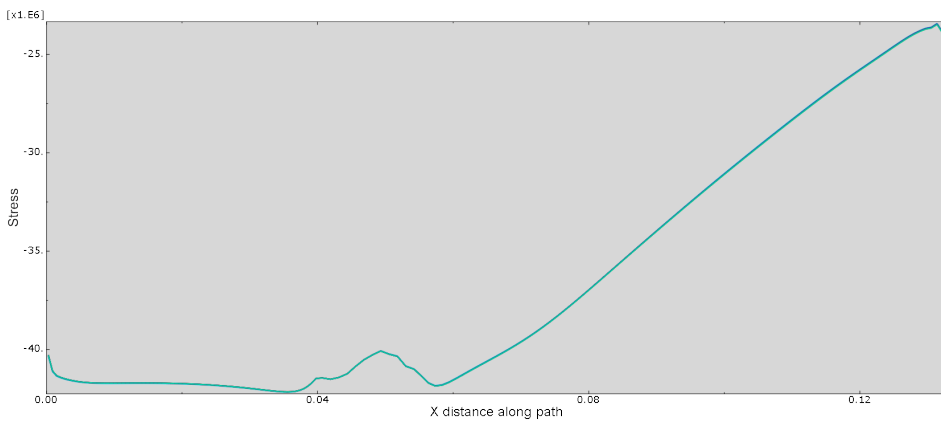
Figure 13: S12 submodel stresses at different plies of the outer skin. The ply is indicated in the caption of each subfigure. Stresses are in Pa, distances in m.



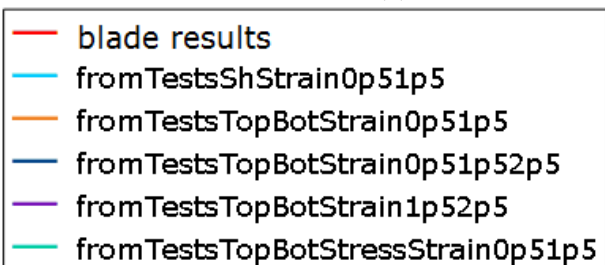
(a) Bottom of ply-1



(b) Top of ply-5



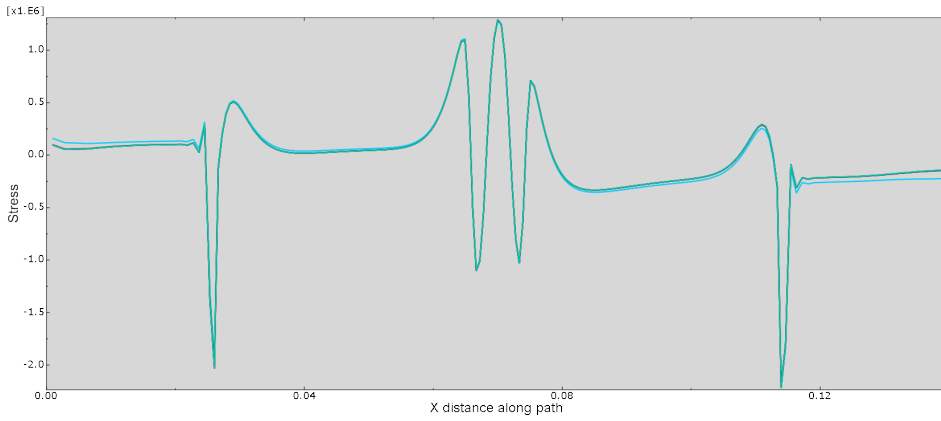
(c) Top of ply-10



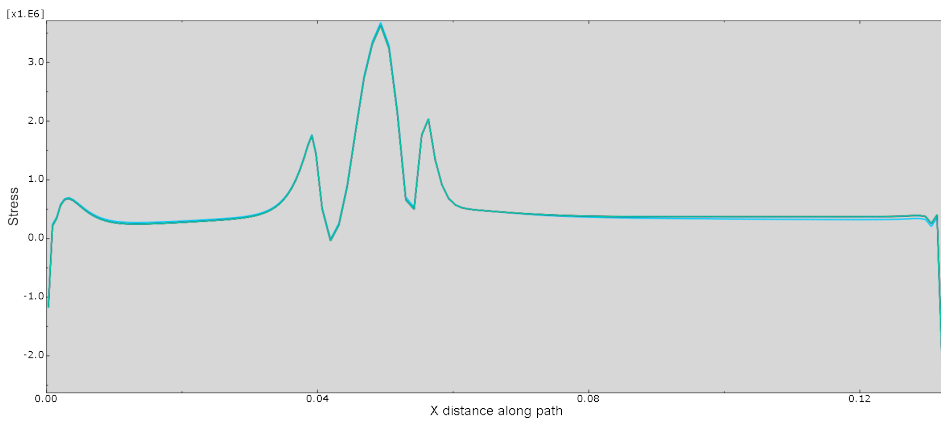
(d) legend

Figure 14: S12 submodel stresses at different plies of the shear web. The ply is indicated in the caption of each subfigure. Stresses are in Pa, distances in m.

Results for the through thickness stresses (S33) are provided below



(a) S33 submodel stresses next to the glue on the outer skin side of the glue

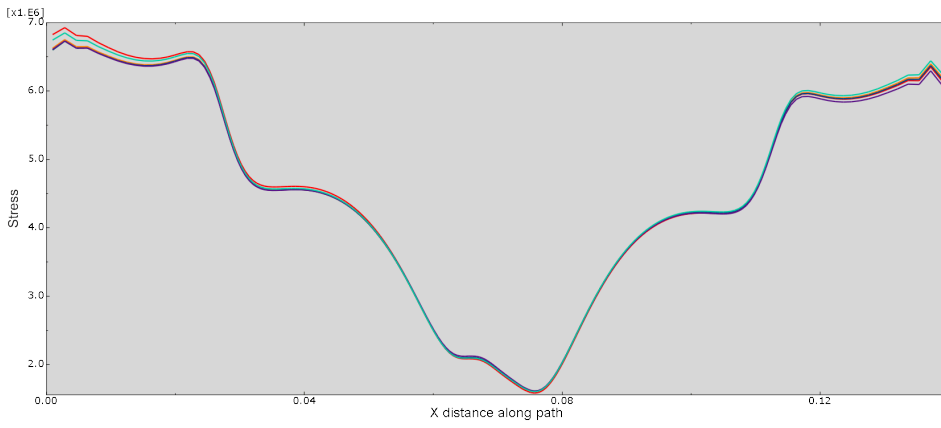


(b) S33 submodel stresses next to the glue on the shear web side of the glue

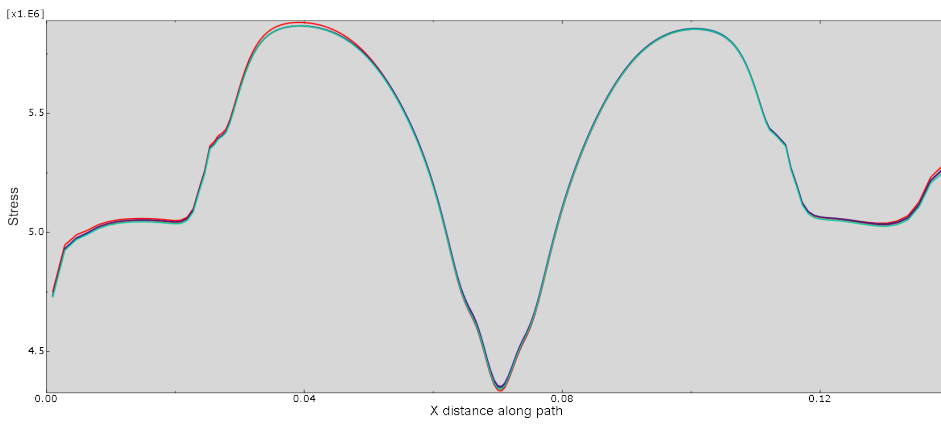
Figure 15: Submodel through thickness stresses. Stresses are in Pa, distances in m.

4.2 Results from extruded profile blade at location 2

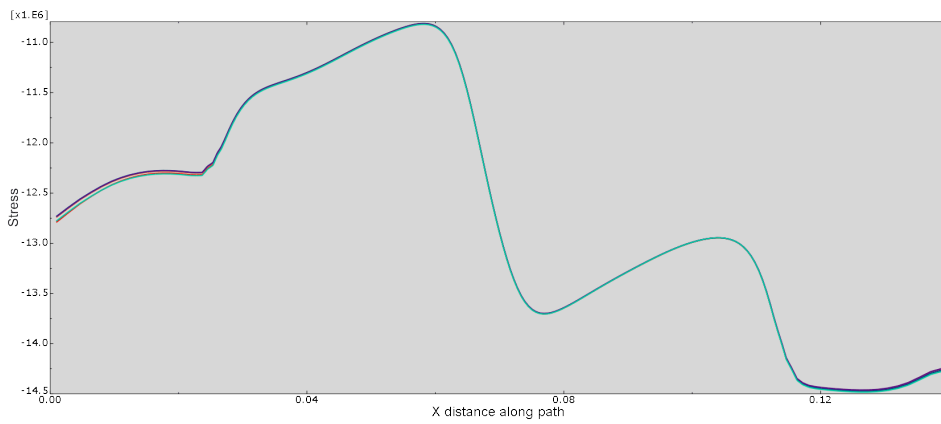
Results for the location 2 in figure 8 are displayed below. The line providing results based on the shell strains (Vector 1 in subsection 3.2), has been removed as the other vectors used to obtain α coefficients consistently performed better. Results remain good at the second location, particularly at the region where the stresses have been extracted to obtain the vectors in subsection 3.2 (region closest to the T-joint).



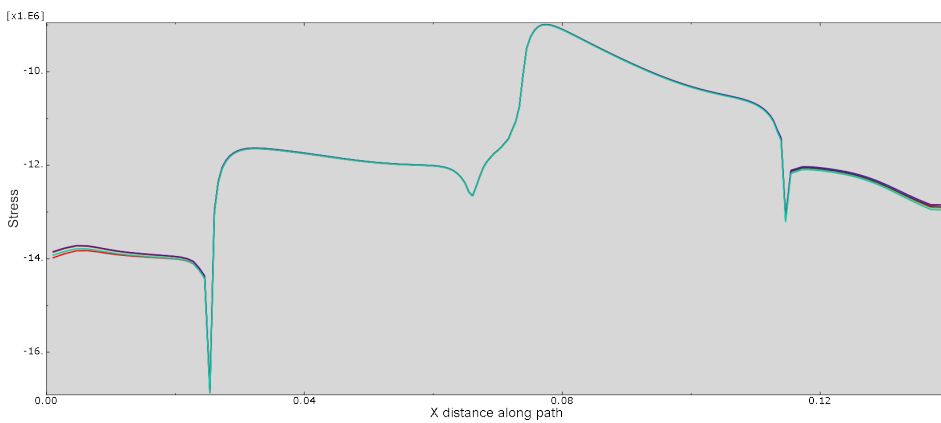
(a) Bottom of ply-1



(b) Middle of ply-5

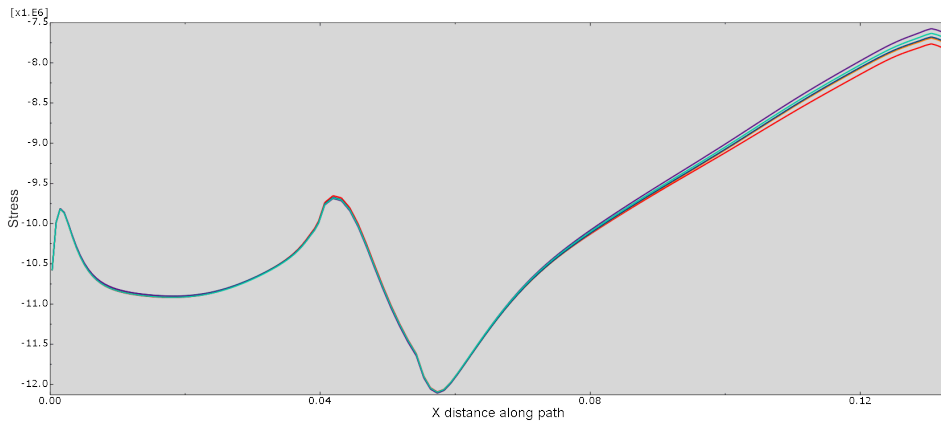


(c) Middle of ply-6

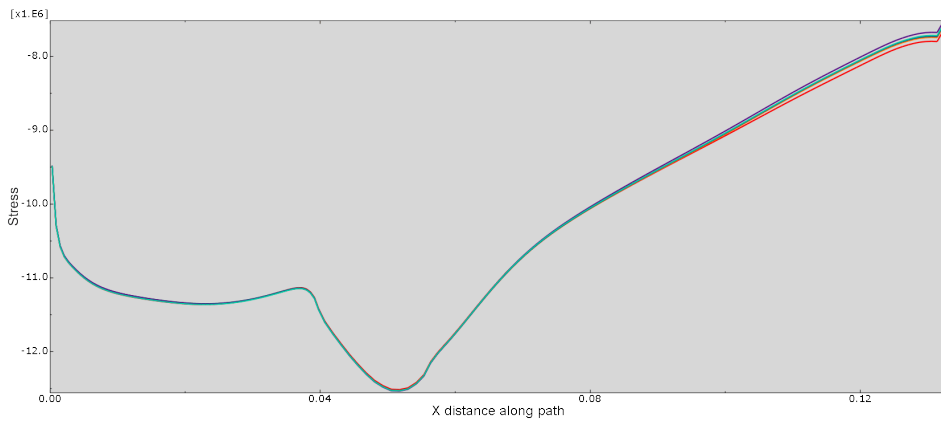


(d) Top of ply 15

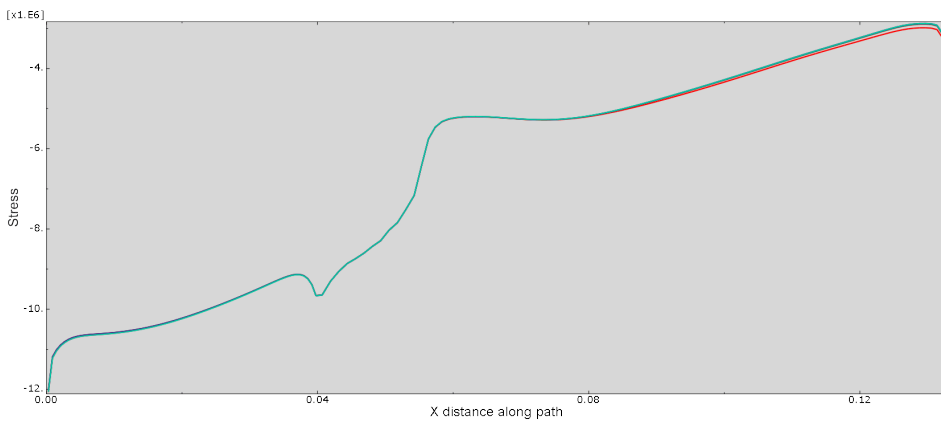
Figure 16: S11 submodel stresses at different plies of the outer skin. The ply is indicated in the caption of each subfigure. Stresses are in Pa, distances in m.



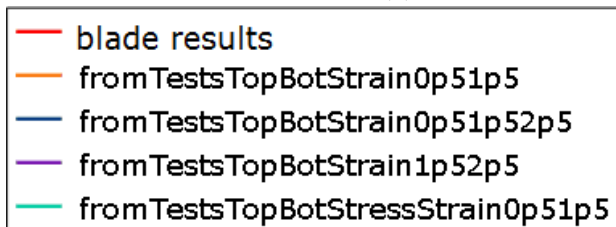
(a) Bottom of ply-1



(b) Top of ply 5

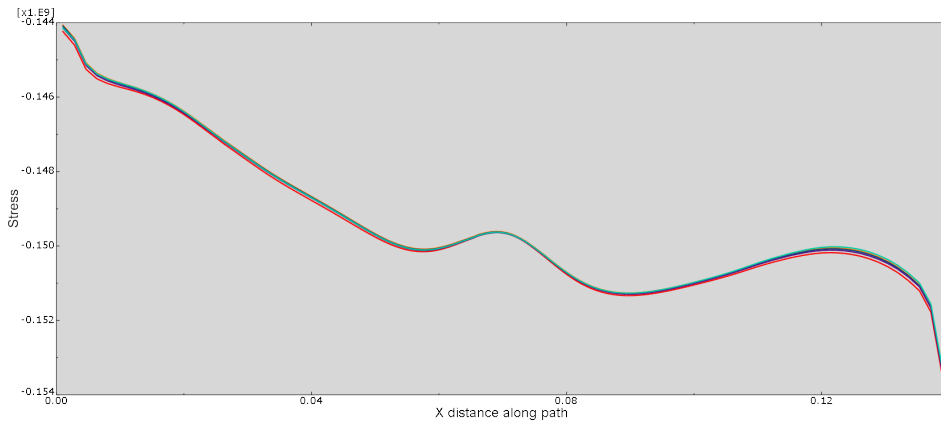


(c) Top of ply 10

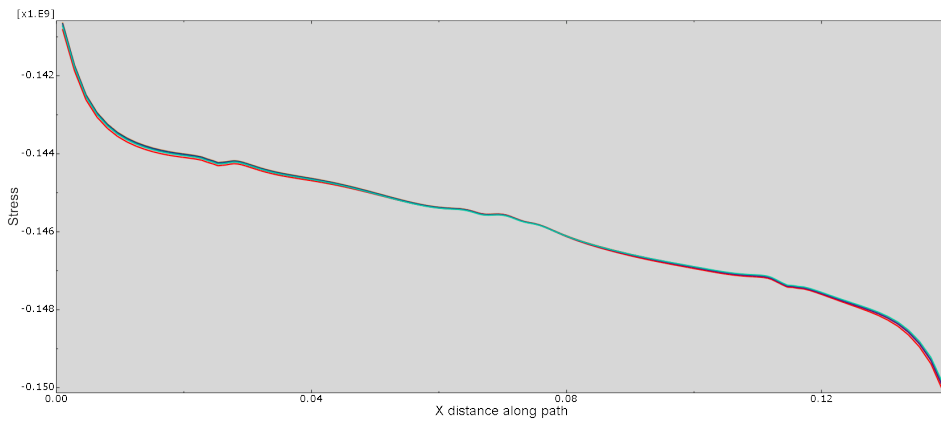


(d) legend

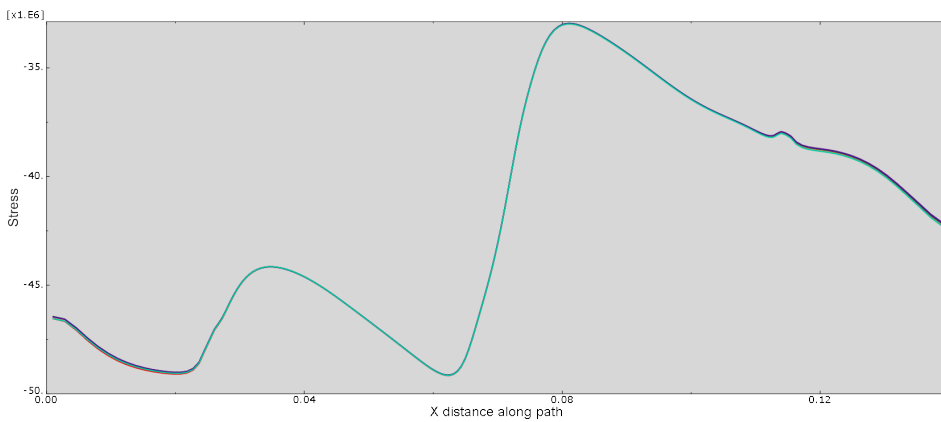
Figure 17: S11 submodel stresses at different plies of the shear web. The ply is indicated in the caption of each subfigure. Stresses are in Pa, distances in m.



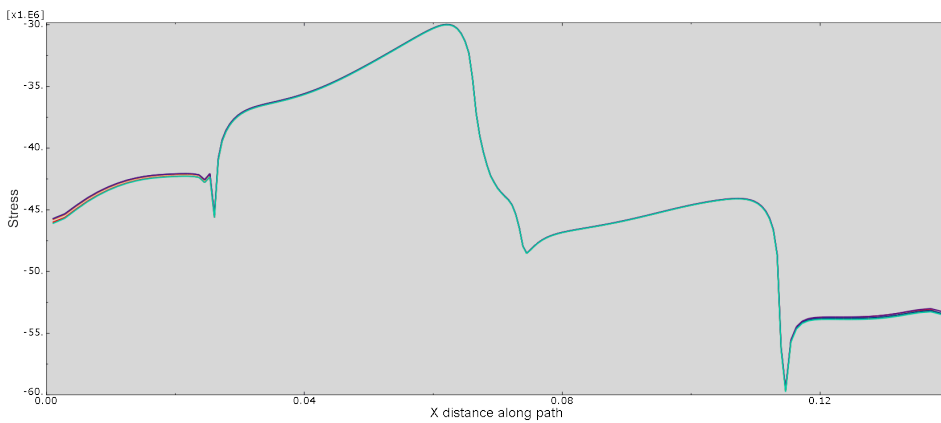
(a) Bottom of ply 1



(b) Middle of ply 5

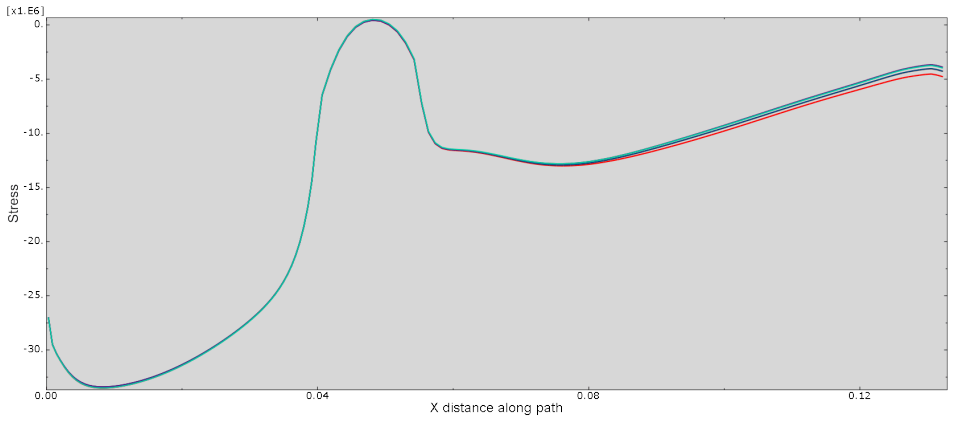


(c) Middle of ply 6

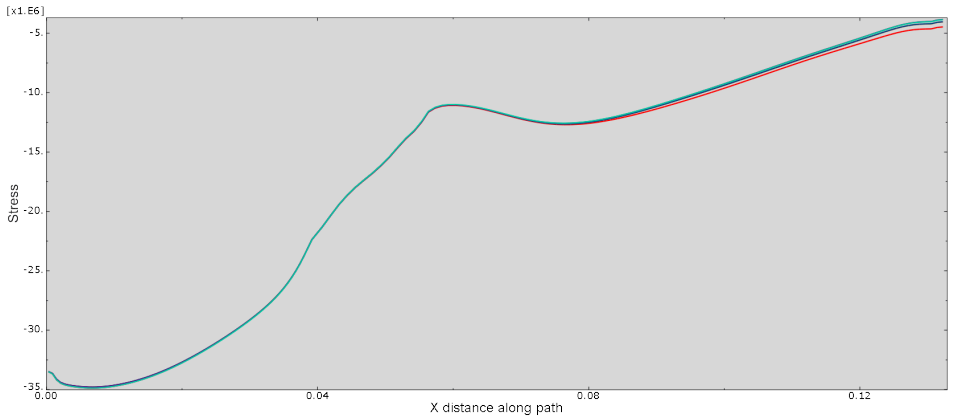


(d) Top of ply 15

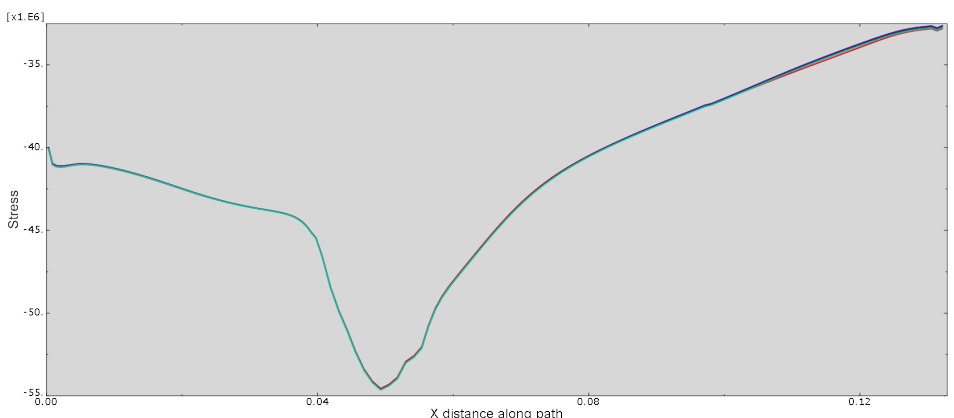
Figure 18: S22 submodel stresses at different plies of the outer skin. The ply is indicated in the caption of each subfigure. Stresses are in Pa, distances in m.



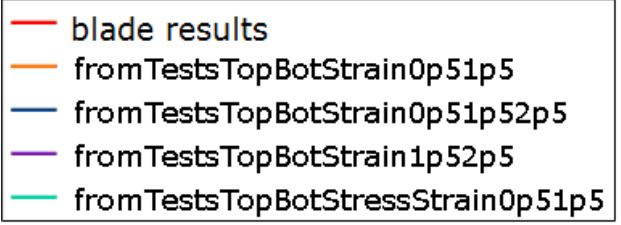
(a) Bottom of ply 1



(b) Top of ply 5

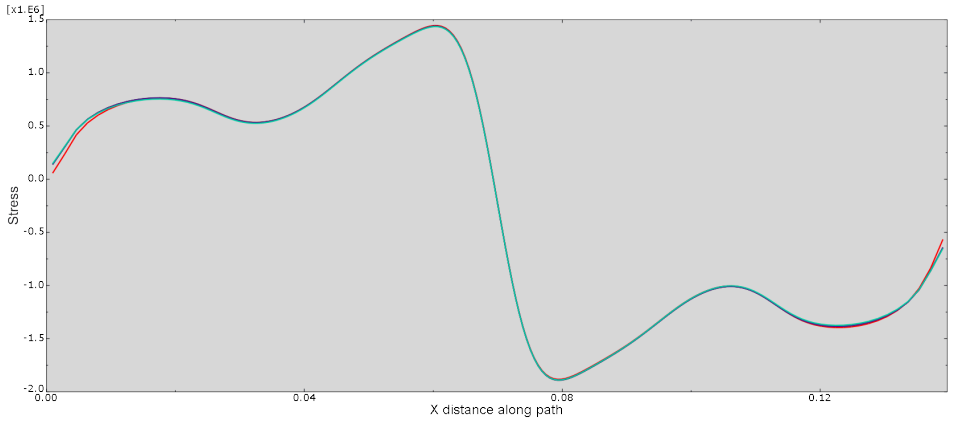


(c) Top of ply 10

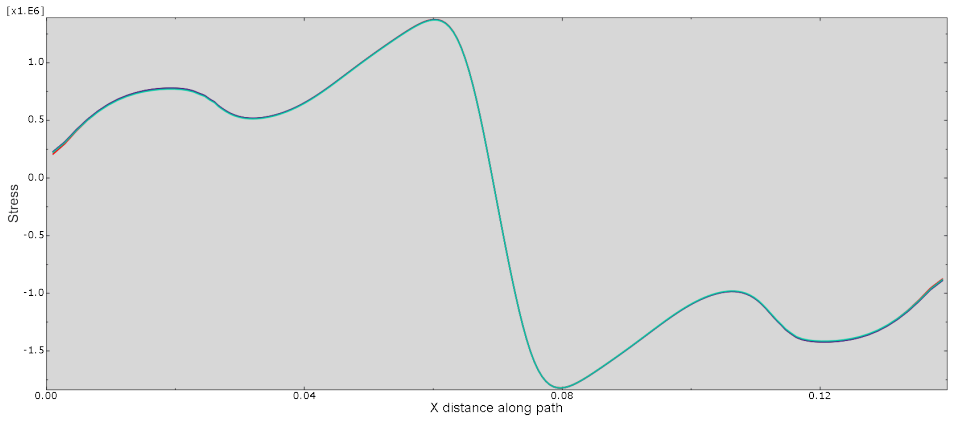


(d) legend

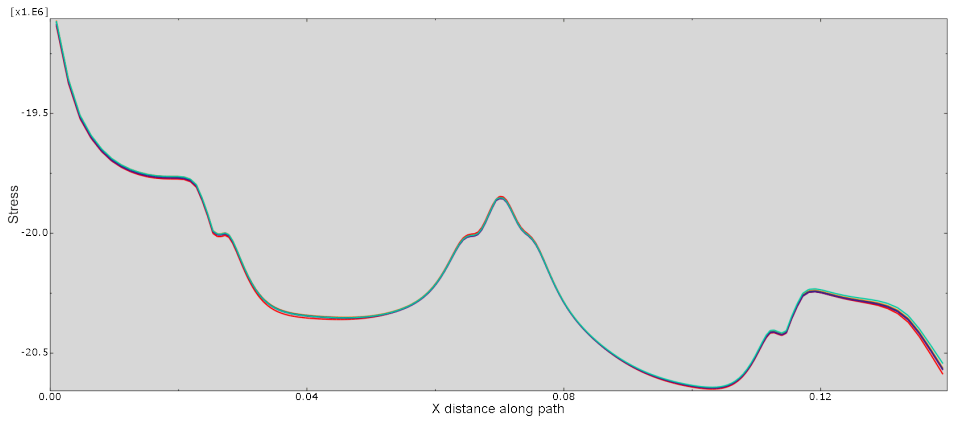
Figure 19: S22 submodel stresses at different plies of the shear web. The ply is indicated in the caption of each subfigure. Stresses are in Pa, distances in m.



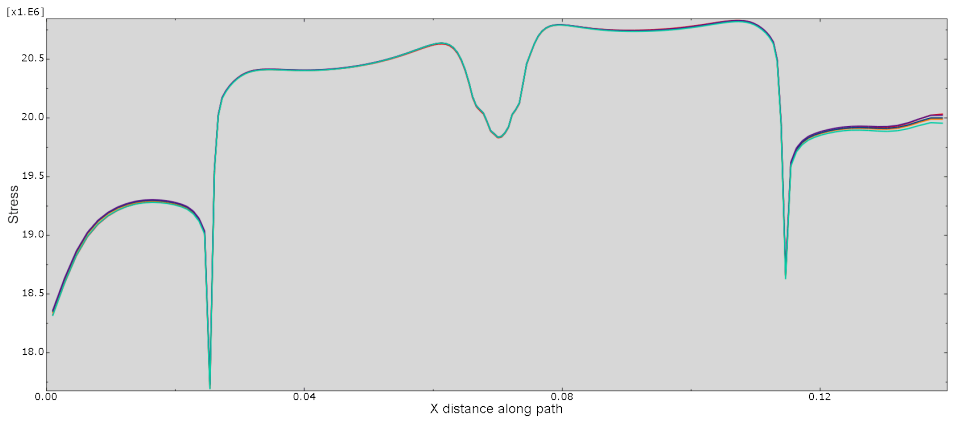
(a) Bottom of ply-1



(b) Middle of ply-5

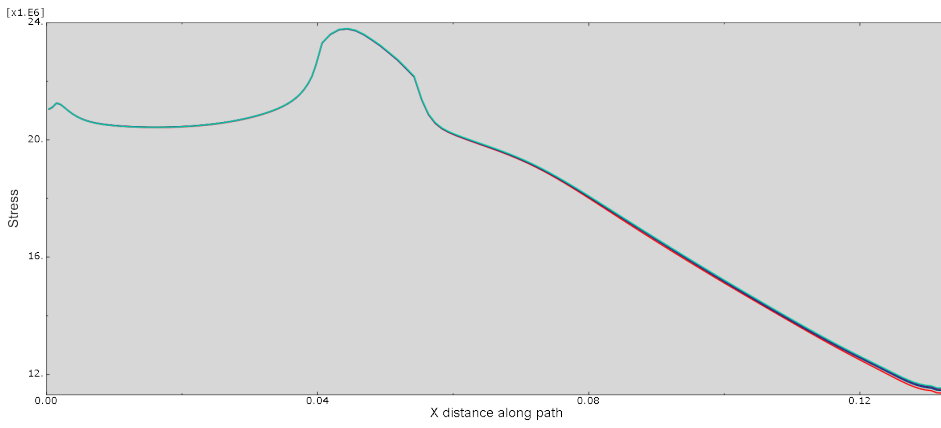


(c) Middle of ply-6

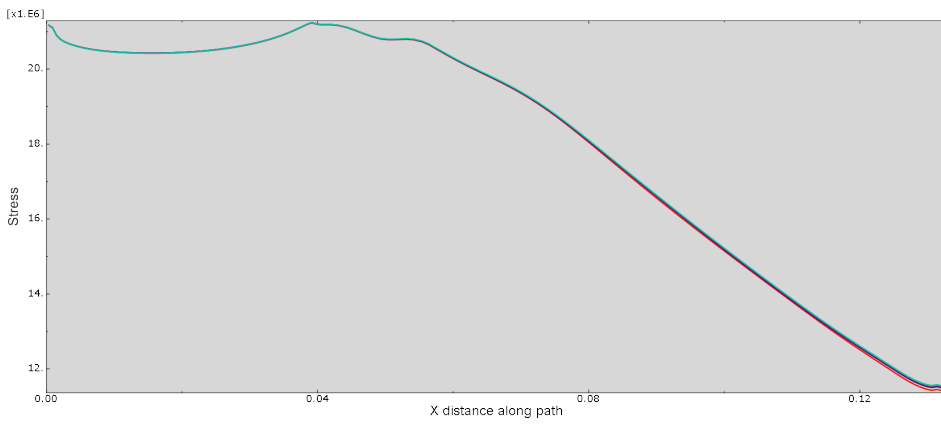


(d) Top of ply-15

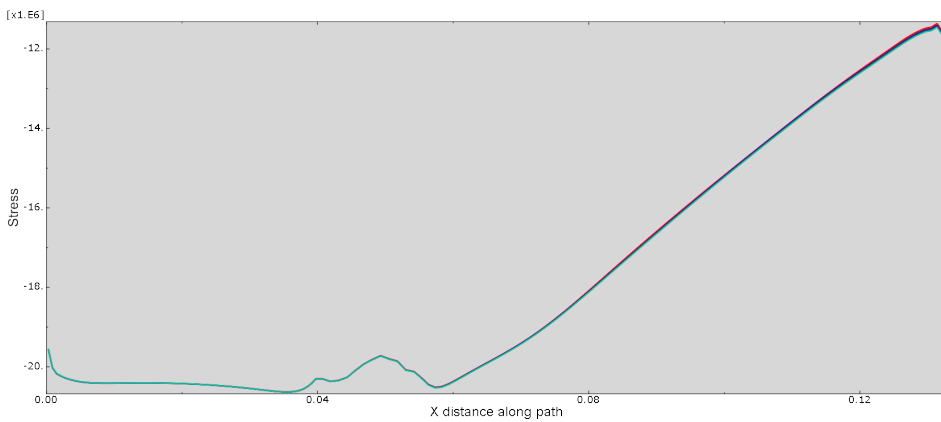
Figure 20: S12 submodel stresses at different plies of the outer skin. The ply is indicated in the caption of each subfigure. Stresses are in Pa, distances in m.



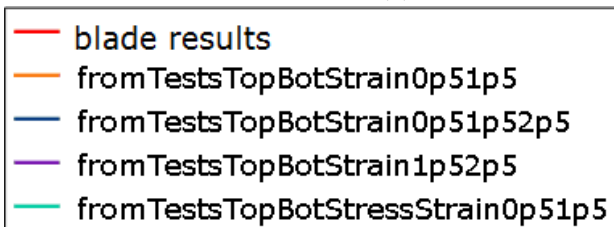
(a) Bottom of ply-1



(b) Top of ply-5



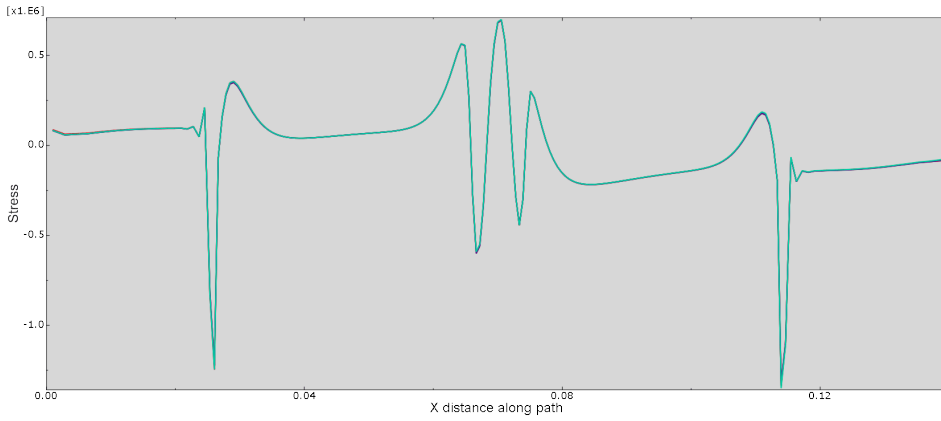
(c) Top of ply-10



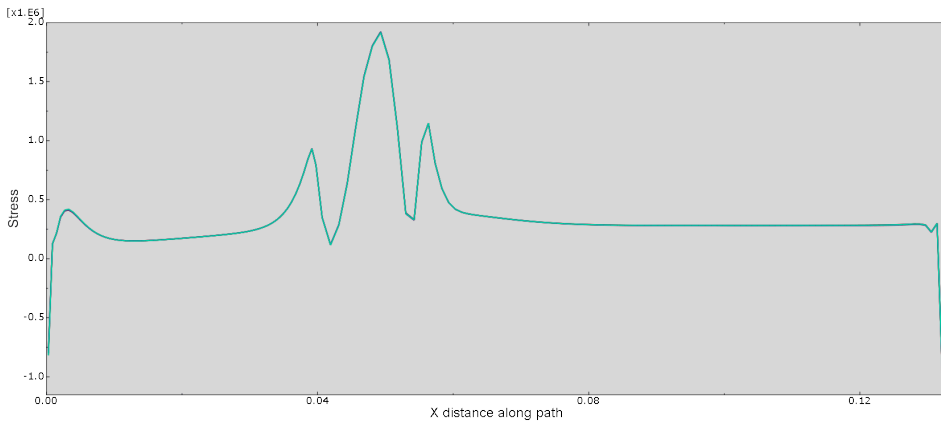
(d) legend

Figure 21: S12 submodel stresses at different plies of the shear web. The ply is indicated in the caption of each subfigure. Stresses are in Pa, distances in m.

Results for the through thickness stresses (S33) are provided below



(a) S33 submodel stresses next to the glue on the outer skin side of the glue

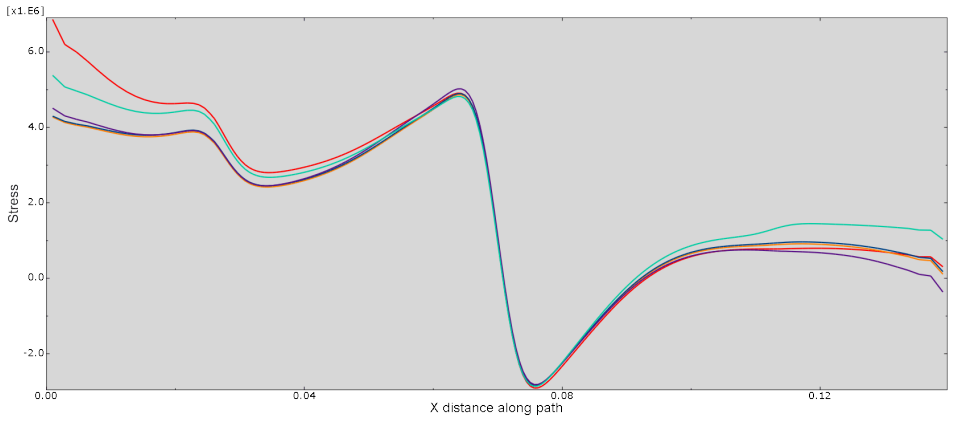


(b) S33 submodel stresses next to the glue on the shear web side of the glue

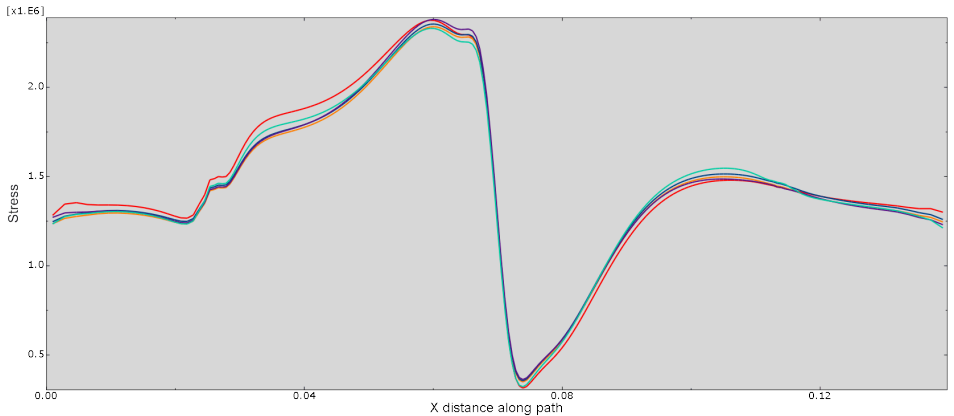
Figure 22: Submodel through thickness stresses. Stresses are in Pa, distances in m.

4.3 Results from twisted blade blade at location 1

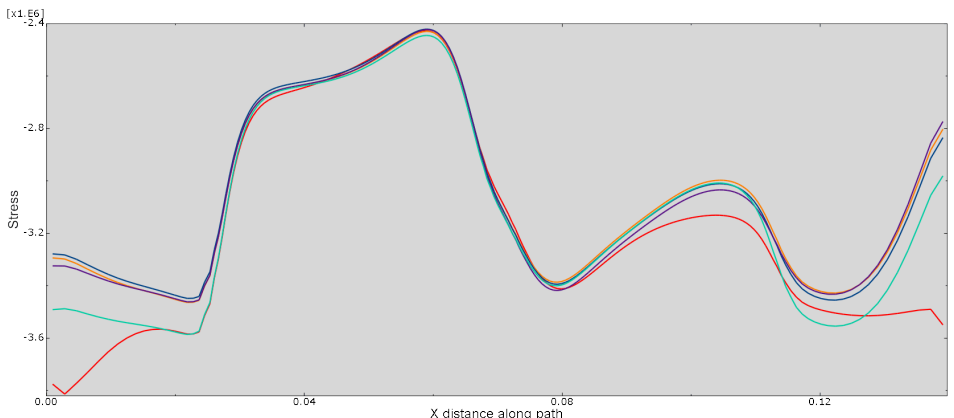
Results for the first location studied on the twisted blade are displayed below. The line providing results based on the shell strains (Vector 1 in subsection 3.2), has been removed as the other vectors used to obtain α coefficients consistently performed better. Results remain good at the first location of the twisted blade, particularly at the region where the stresses have been extracted to obtain the vectors in subsection 3.2 (region closest to the T-joint).



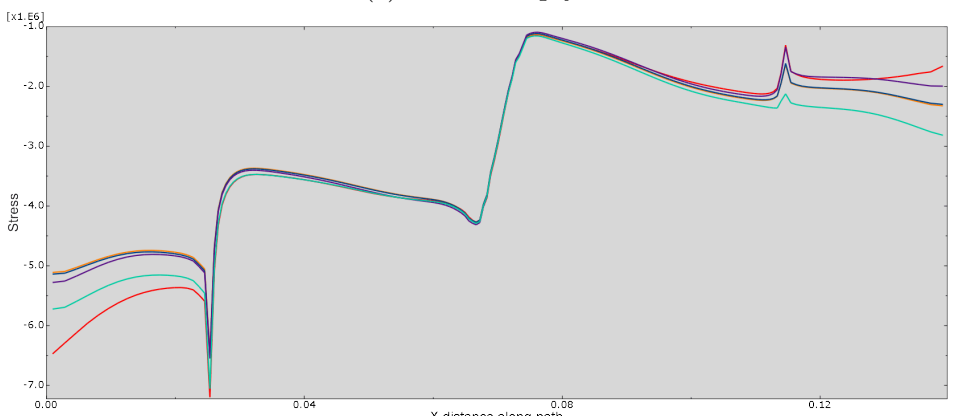
(a) Bottom of ply-1



(b) Middle of ply-5

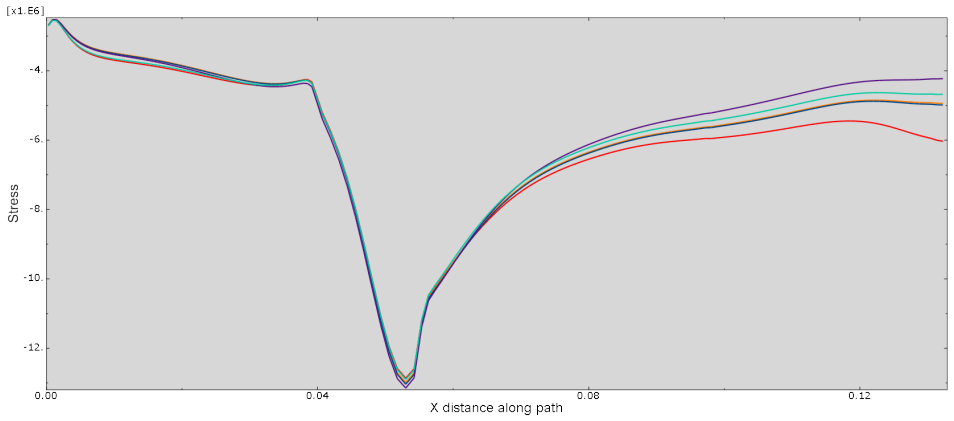


(c) Middle of ply-6

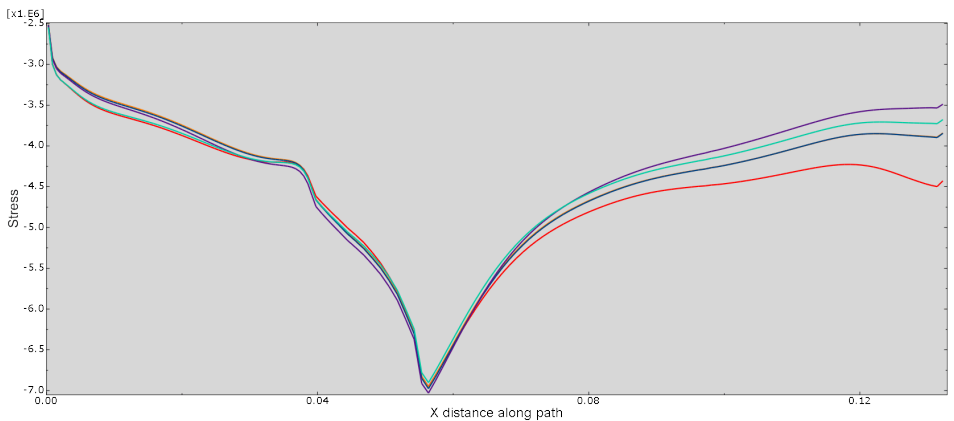


(d) Top of ply 15

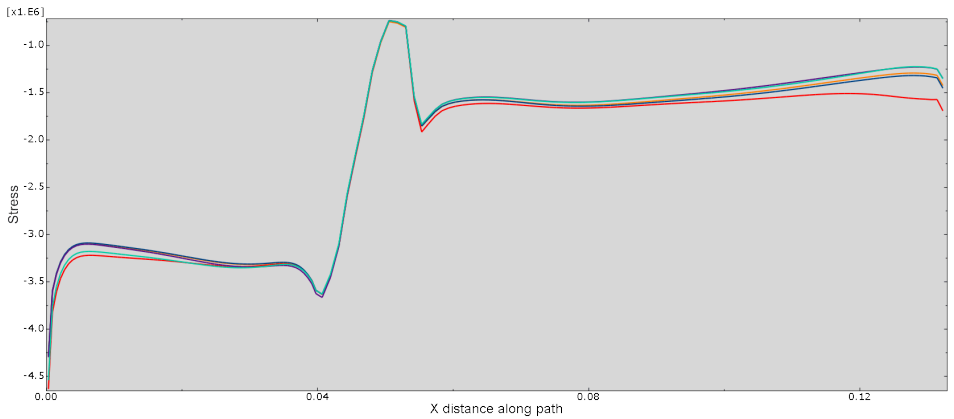
Figure 23: S11 submodel stresses at different plies of the outer skin. The ply is indicated in the caption of each subfigure. Stresses are in Pa, distances in m.



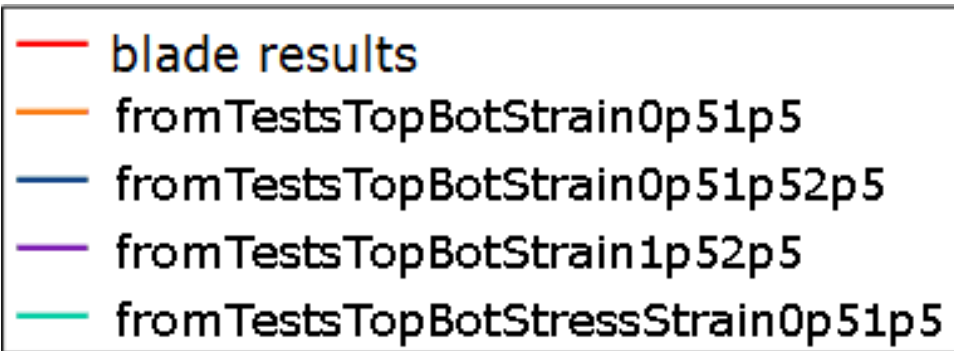
(a) Bottom of ply-1



(b) Top of ply 5

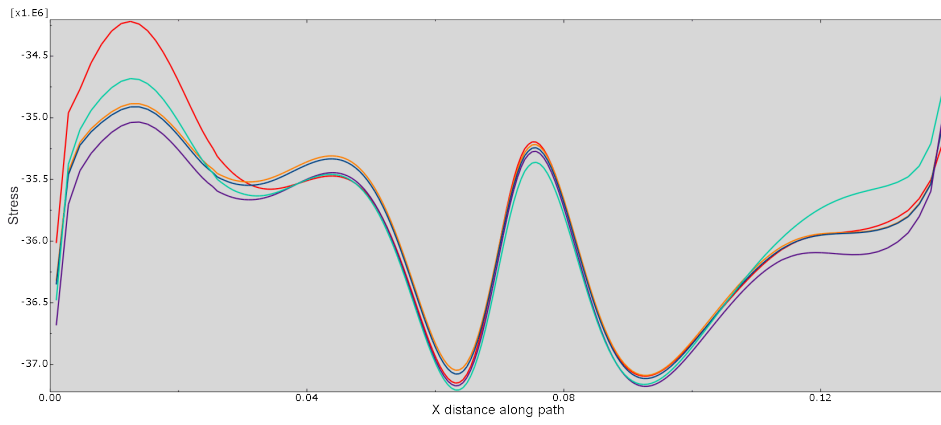


(c) Top of ply 10

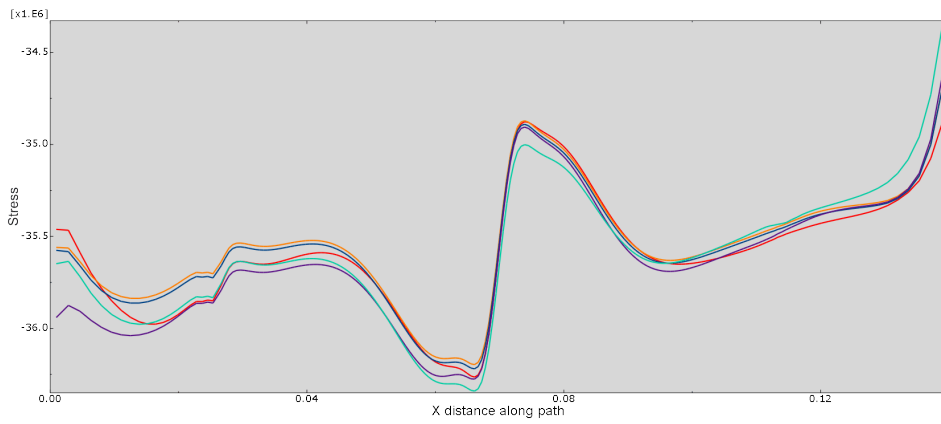


(d) legend

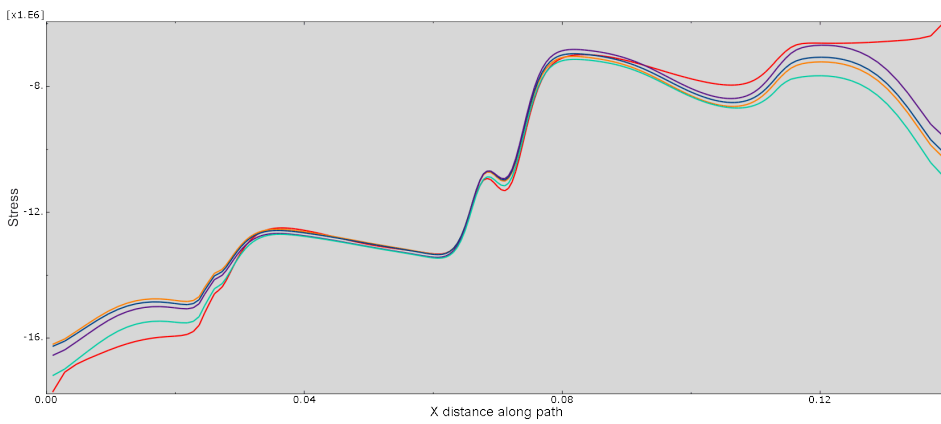
Figure 24: S11 submodel stresses at different plies of the shear web. The ply is indicated in the caption of each subfigure. Stresses are in Pa, distances in m.



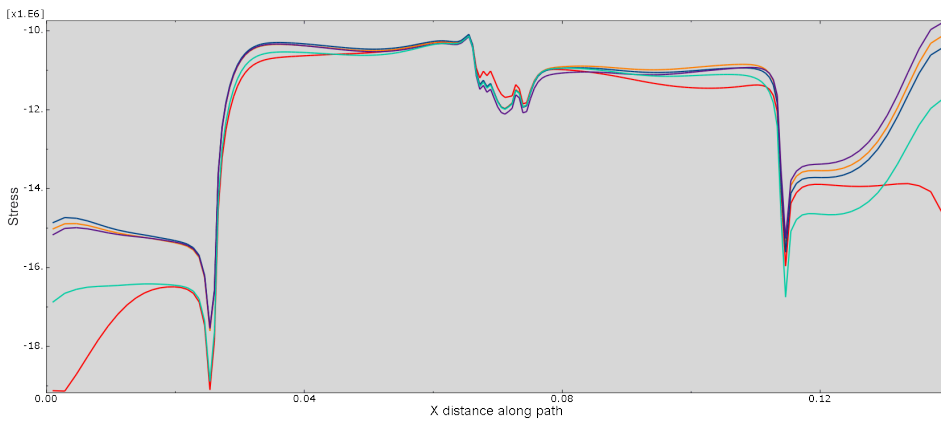
(a) Bottom of ply 1



(b) Middle of ply 5

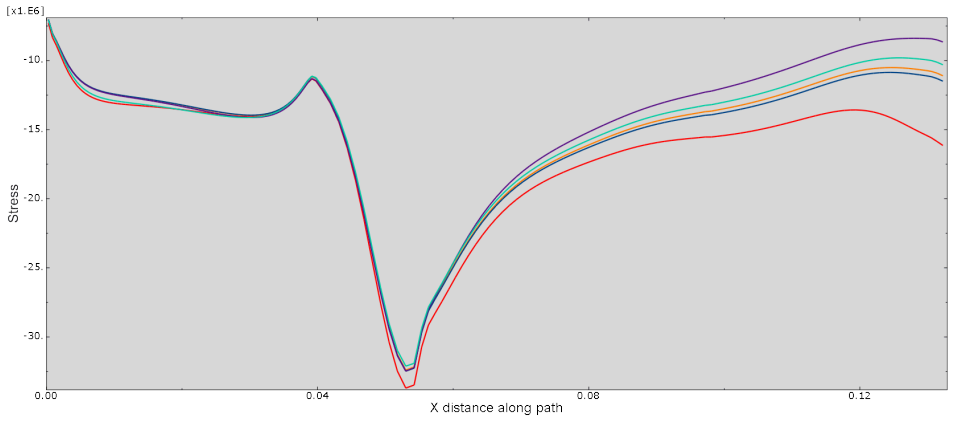


(c) Middle of ply 6

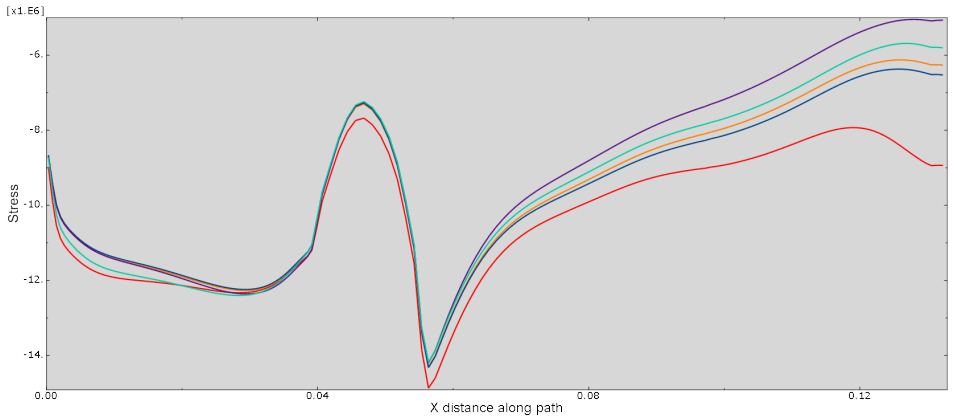


(d) Top of ply 15

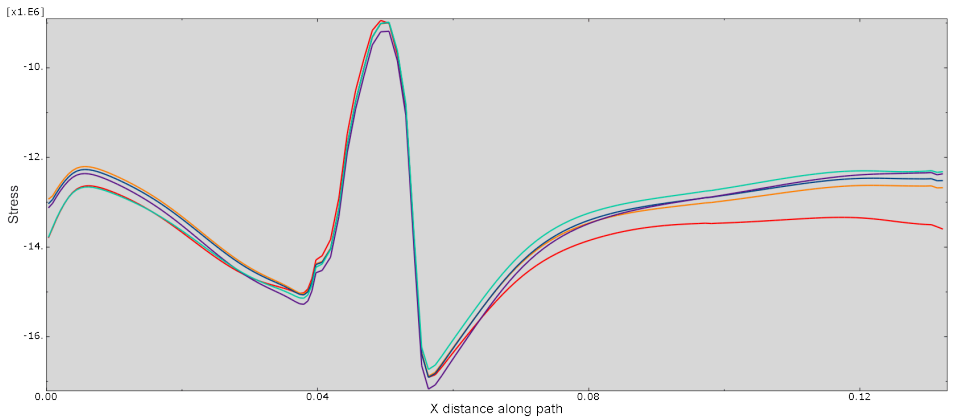
Figure 25: S22 submodel stresses at different plies of the outer skin. The ply is indicated in the caption of each subfigure. Stresses are in Pa, distances in m.



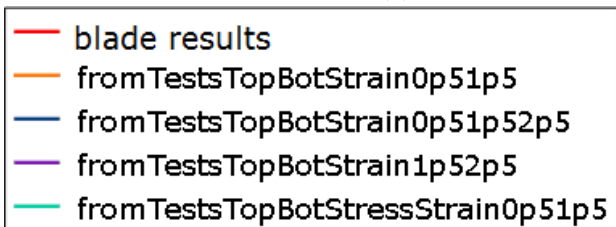
(a) Bottom of ply 1



(b) Top of ply 5

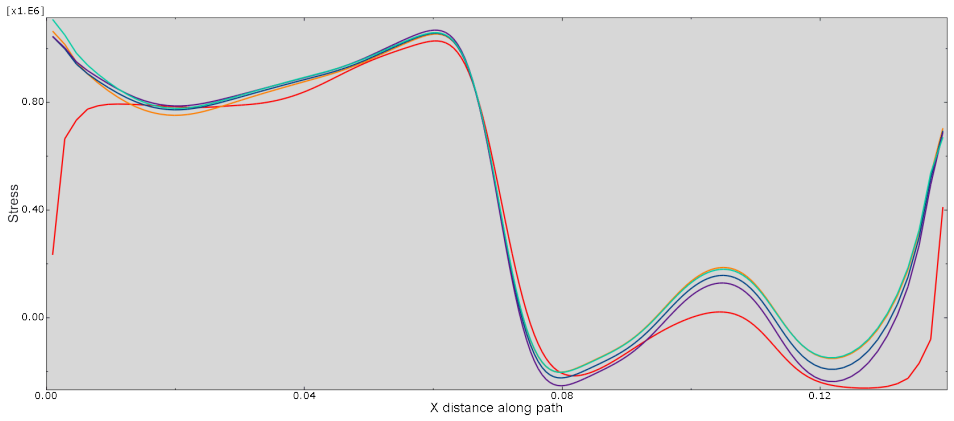


(c) Top of ply 10

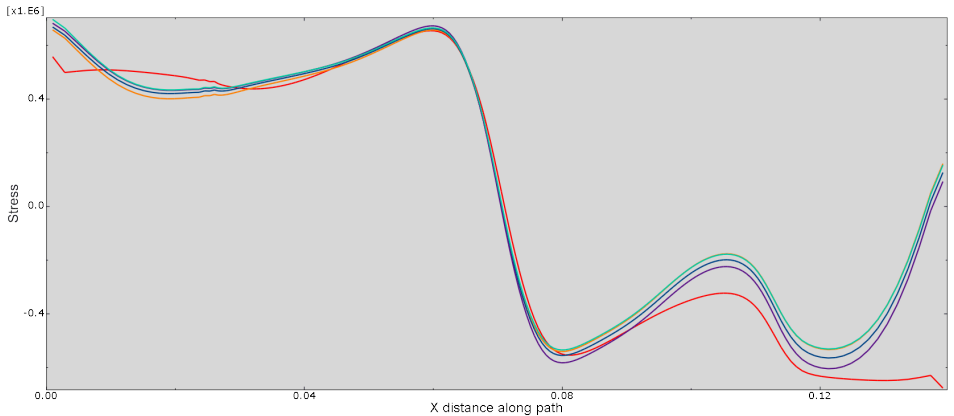


(d) legend

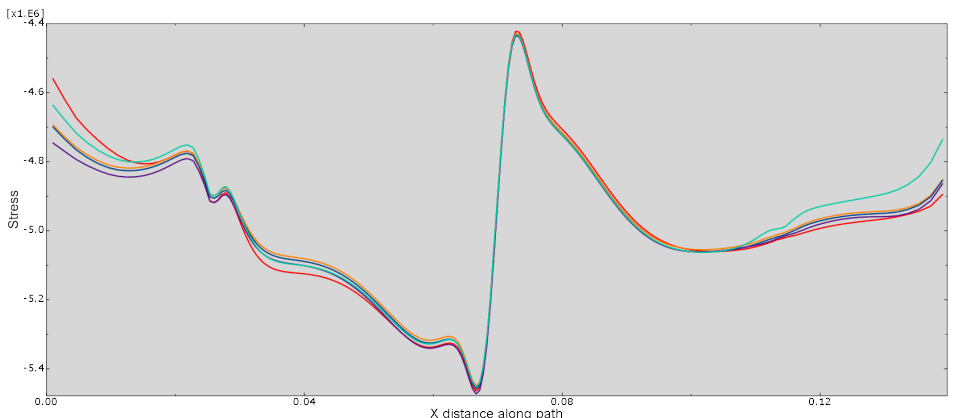
Figure 26: S22 submodel stresses at different plies of the shear web. The ply is indicated in the caption of each subfigure. Stresses are in Pa, distances in m.



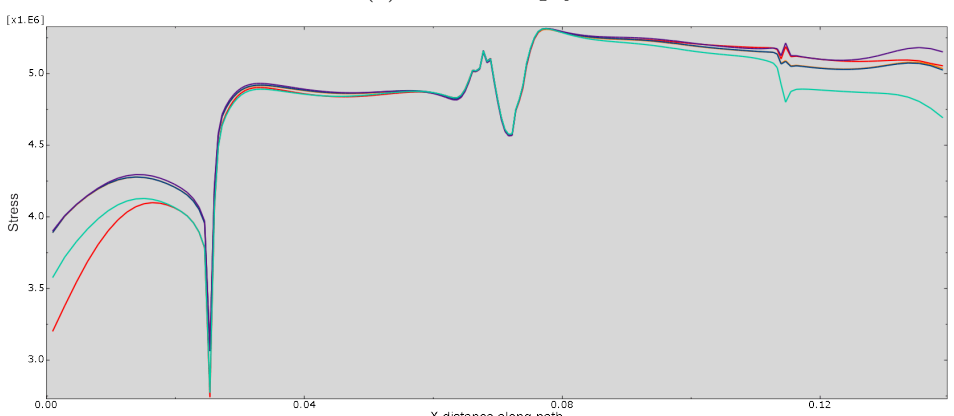
(a) Bottom of ply-1



(b) Middle of ply-5

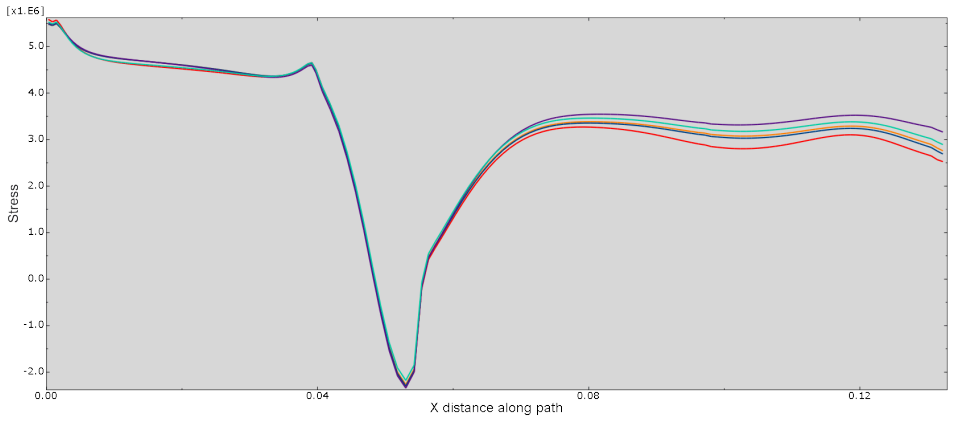


(c) Middle of ply-6

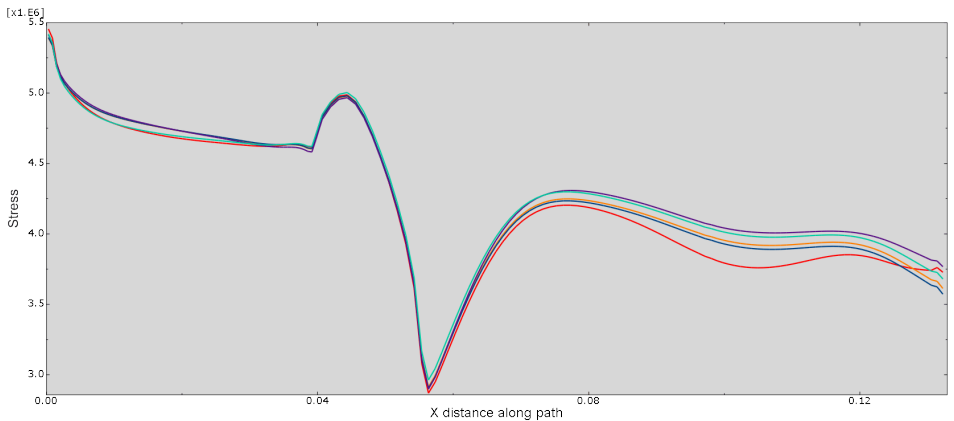


(d) Top of ply-15

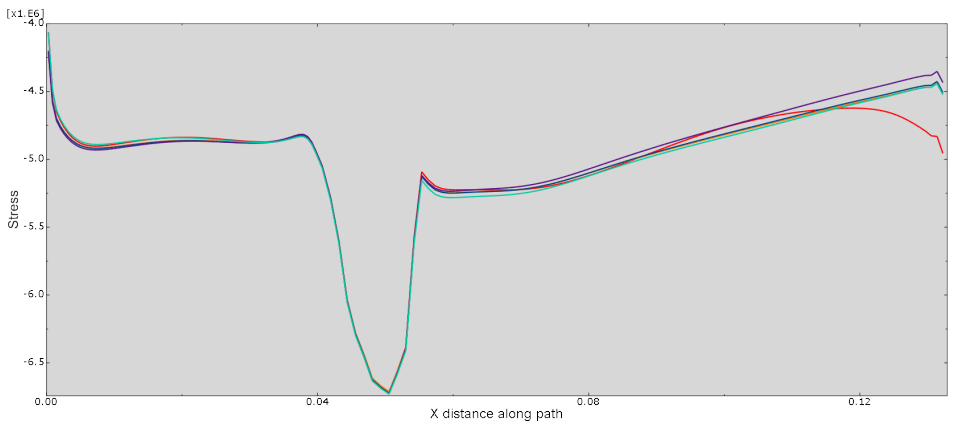
Figure 27: S12 submodel stresses at different plies of the outer skin. The ply is indicated in the caption of each subfigure. Stresses are in Pa, distances in m.



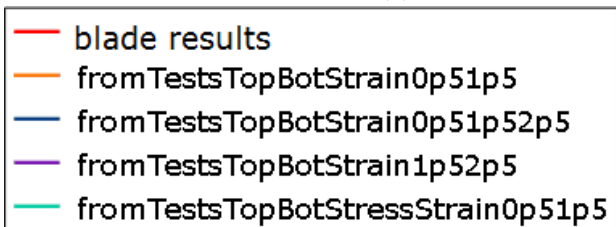
(a) Bottom of ply-1



(b) Top of ply-5



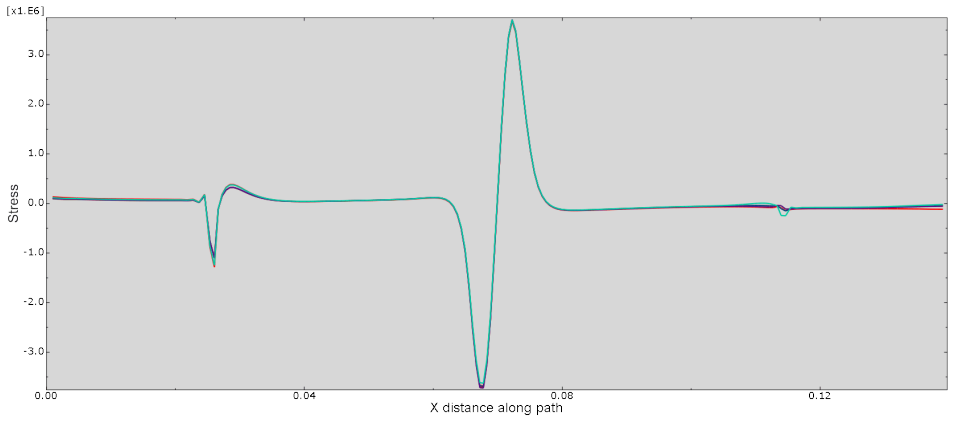
(c) Top of ply-10



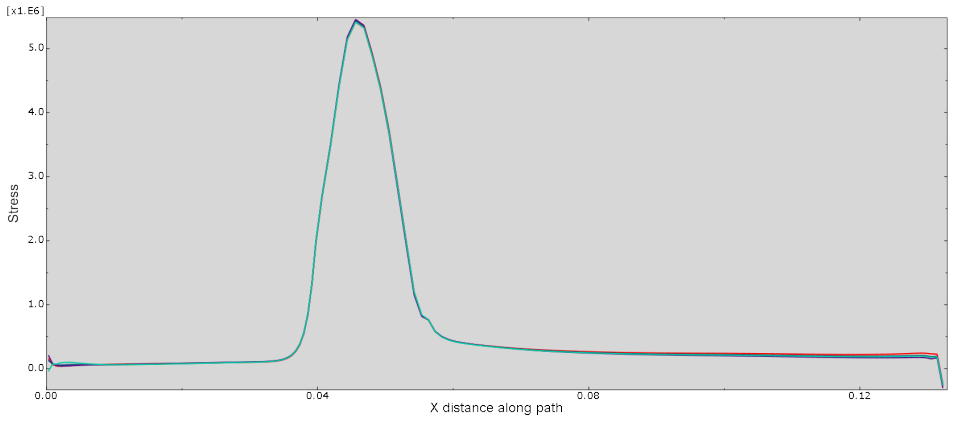
(d) legend

Figure 28: S12 submodel stresses at different plies of the shear web. The ply is indicated in the caption of each subfigure. Stresses are in Pa, distances in m.

Results for the through thickness stresses (S33) are provided below



(a) S33 submodel stresses next to the glue on the outer skin side of the glue

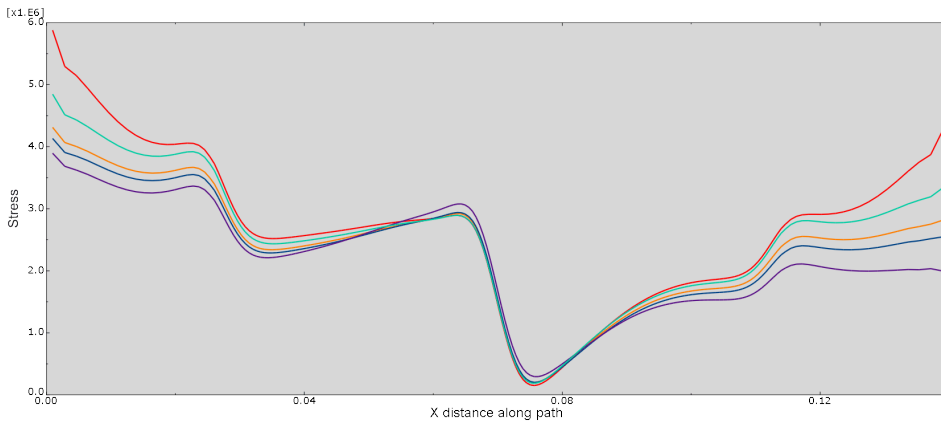


(b) S33 submodel stresses next to the glue on the shear web side of the glue. Stresses are in Pa, distances in m.

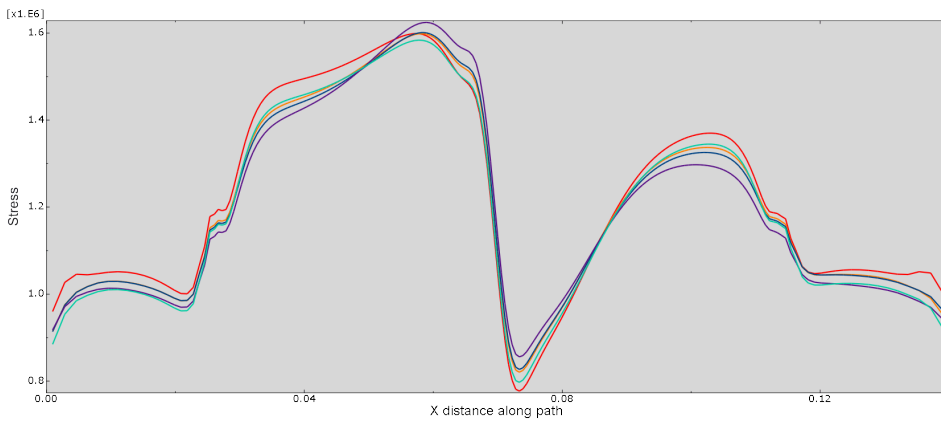
Figure 29: Submodel through thickness stresses

4.4 Results from twisted blade blade at location 2

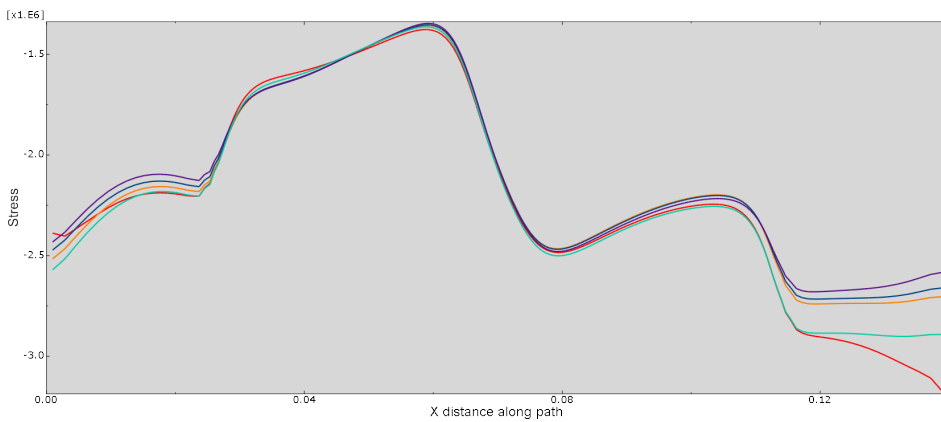
Results for the second location studied on the twisted blade are displayed below. The line providing results based on the shell strains (Vector 1 in subsection 3.2), has been removed as the other vectors used to obtain α coefficients consistently performed better. Results remain good at the second location, particularly at the region where the stresses have been extracted to obtain the vectors in subsection 3.2 (region closest to the T-joint).



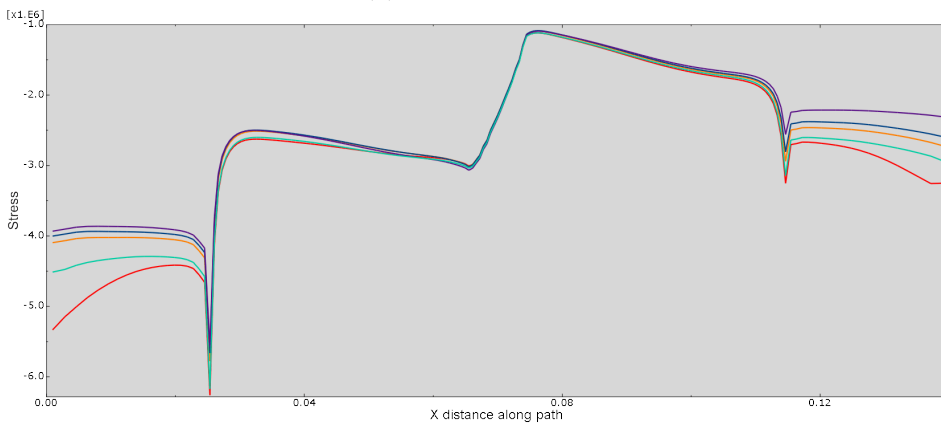
(a) Bottom of ply-1



(b) Middle of ply-5

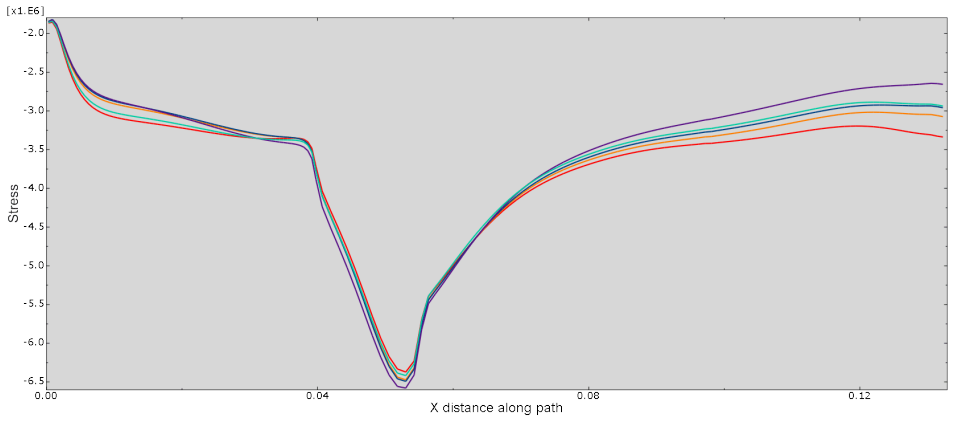


(c) Middle of ply-6

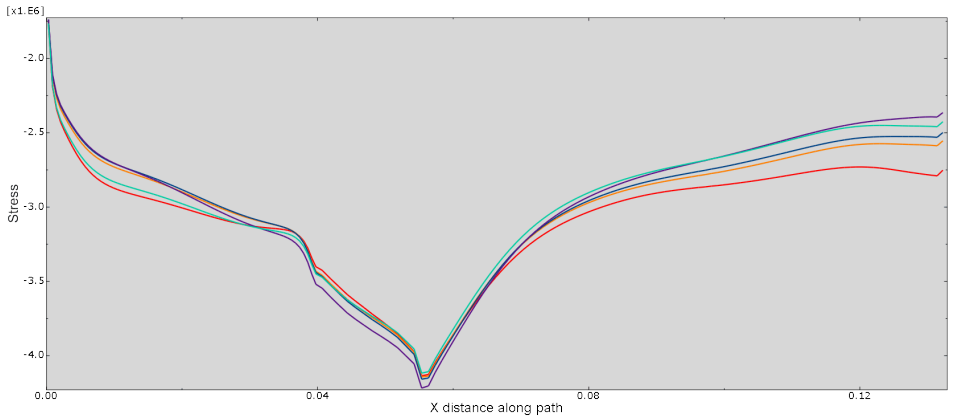


(d) Top of ply 15

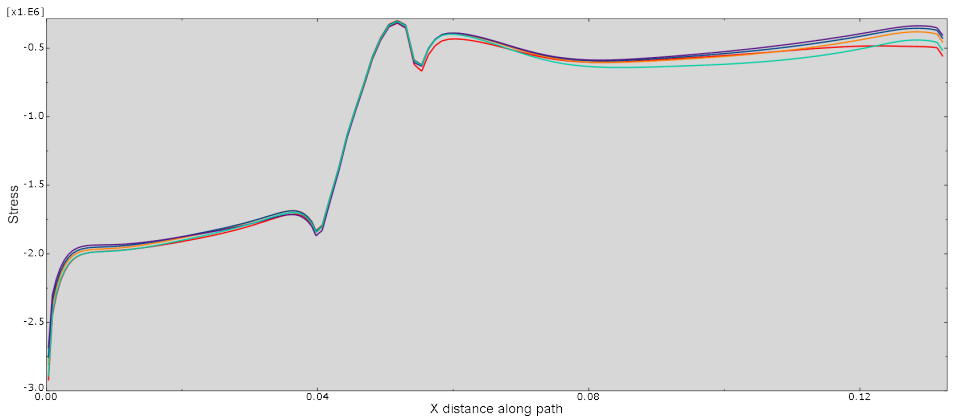
Figure 30: S11 submodel stresses at different plies of the outer skin. The ply is indicated in the caption of each subfigure. Stresses are in Pa, distances in m.



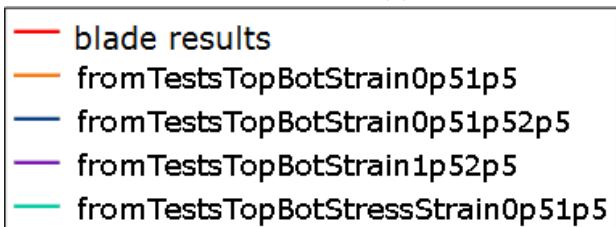
(a) Bottom of ply-1



(b) Top of ply 5

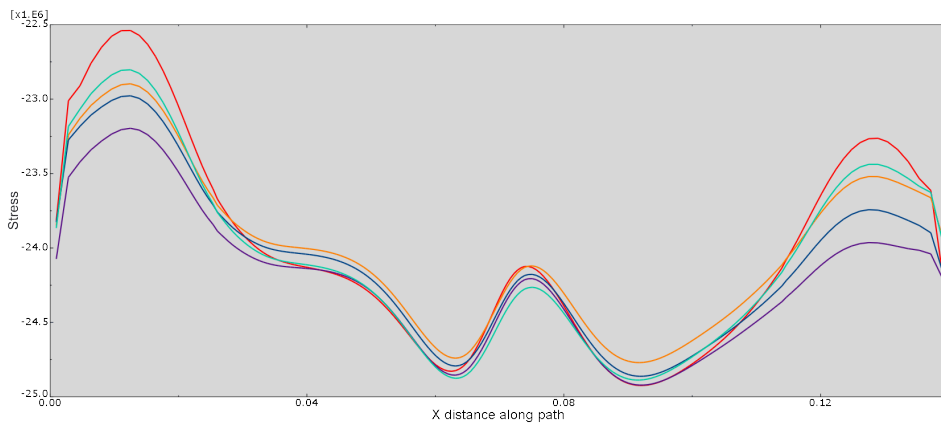


(c) Top of ply 10

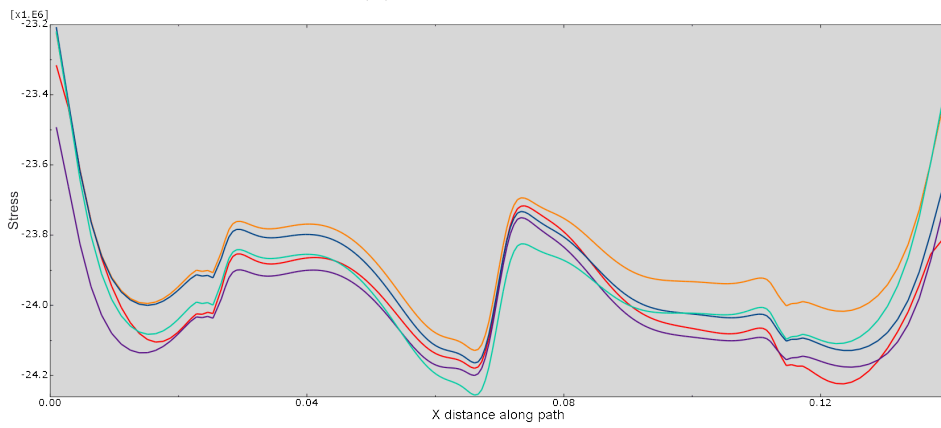


(d) legend

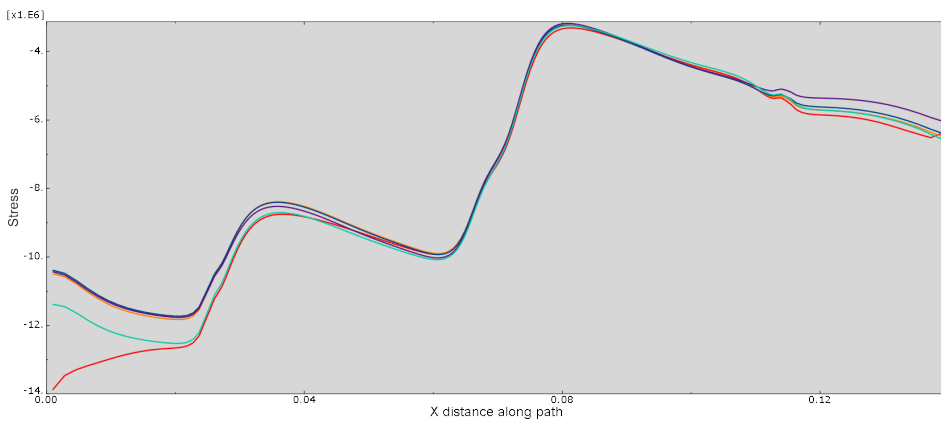
Figure 31: S11 submodel stresses at different plies of the shear web. The ply is indicated in the caption of each subfigure. Stresses are in Pa, distances in m.



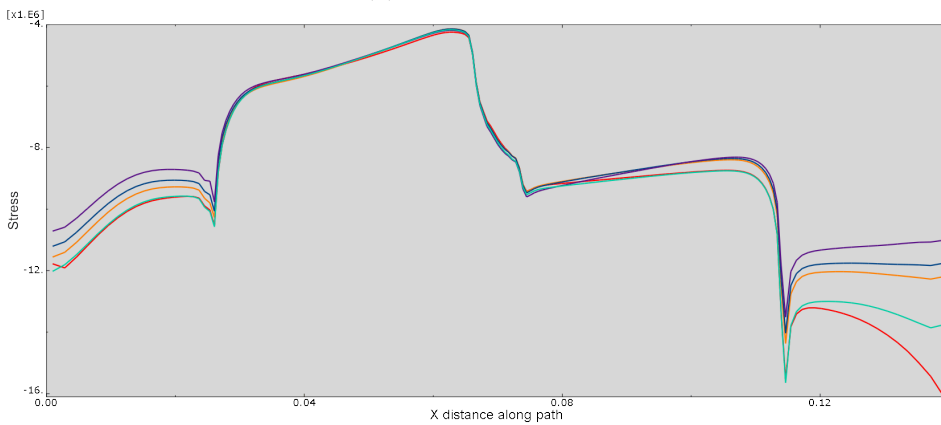
(a) Bottom of ply 1



(b) Middle of ply 5

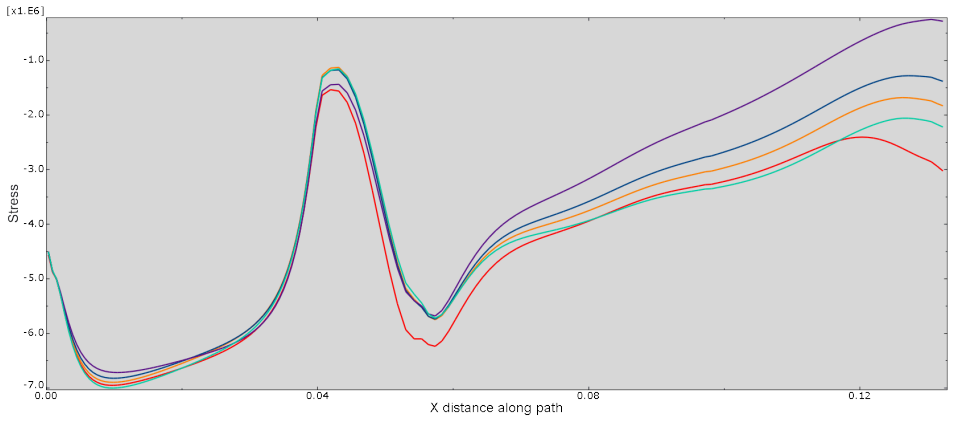


(c) Middle of ply 6

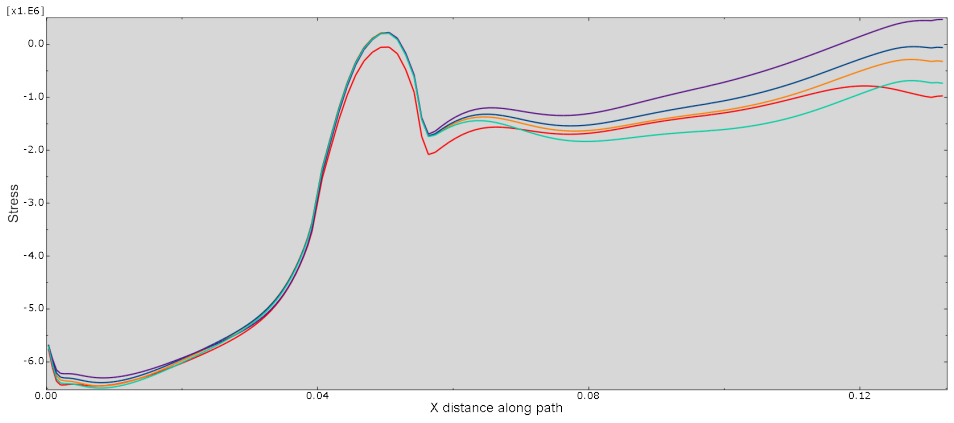


(d) Top of ply 15

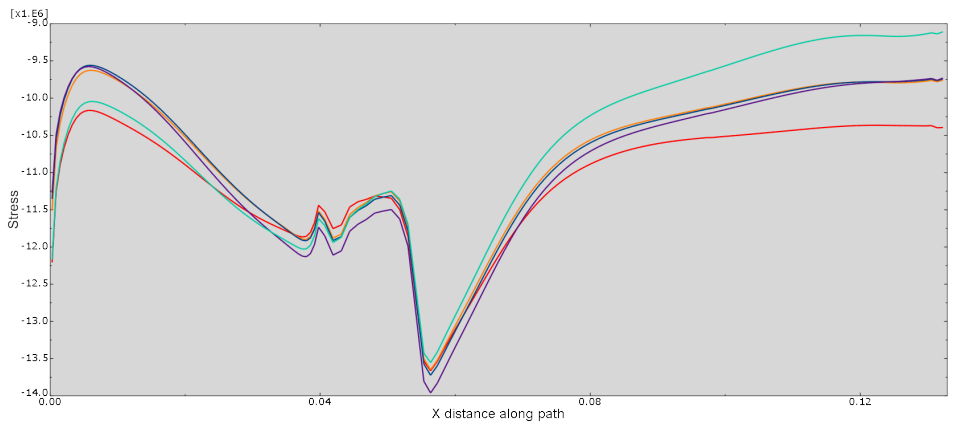
Figure 32: S22 submodel stresses at different plies of the outer skin. The ply is indicated in the caption of each subfigure. Stresses are in Pa, distances in m.



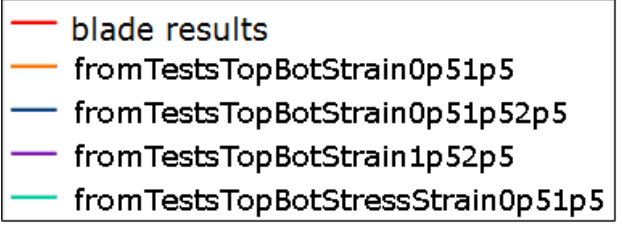
(a) Bottom of ply 1



(b) Top of ply 5

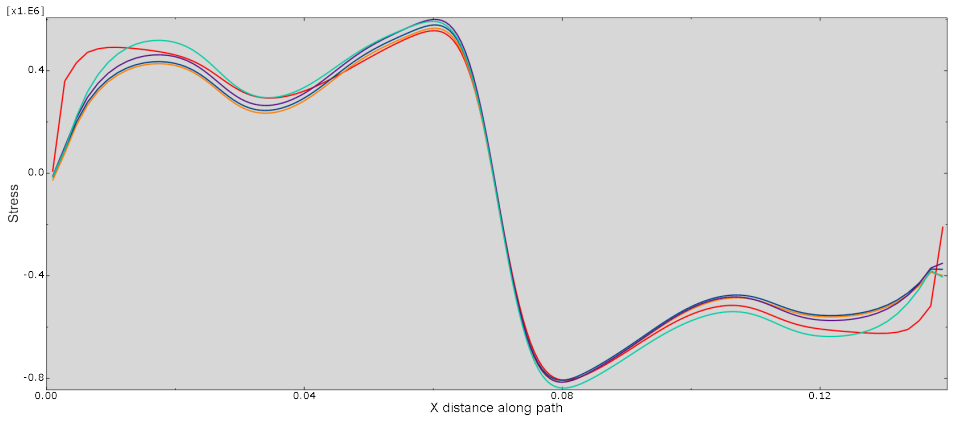


(c) Top of ply 10

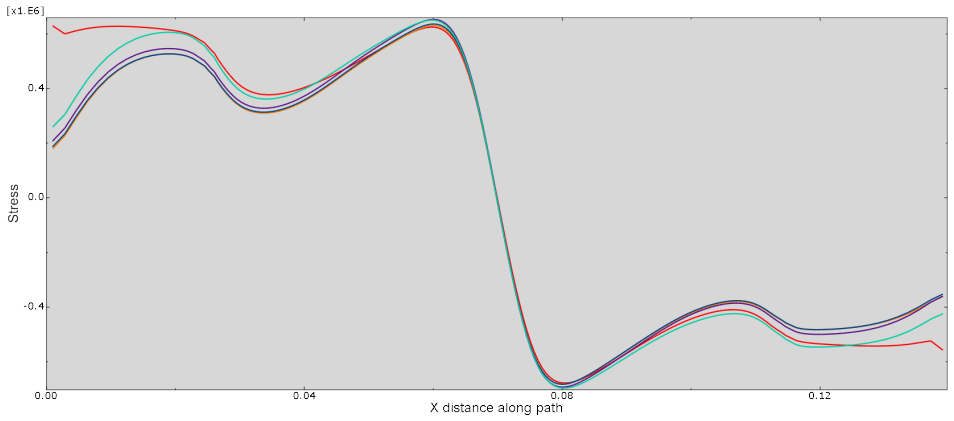


(d) legend

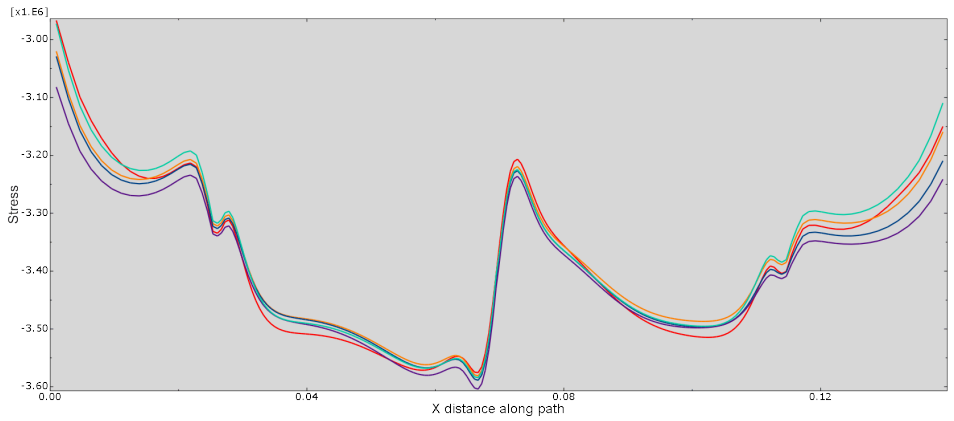
Figure 33: S22 submodel stresses at different plies of the shear web. The ply is indicated in the caption of each subfigure. Stresses are in Pa, distances in m.



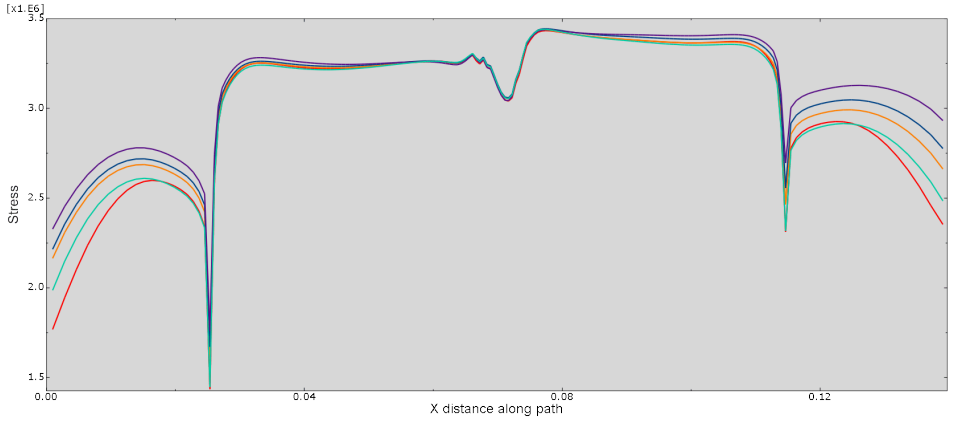
(a) Bottom of ply-1



(b) Middle of ply-5

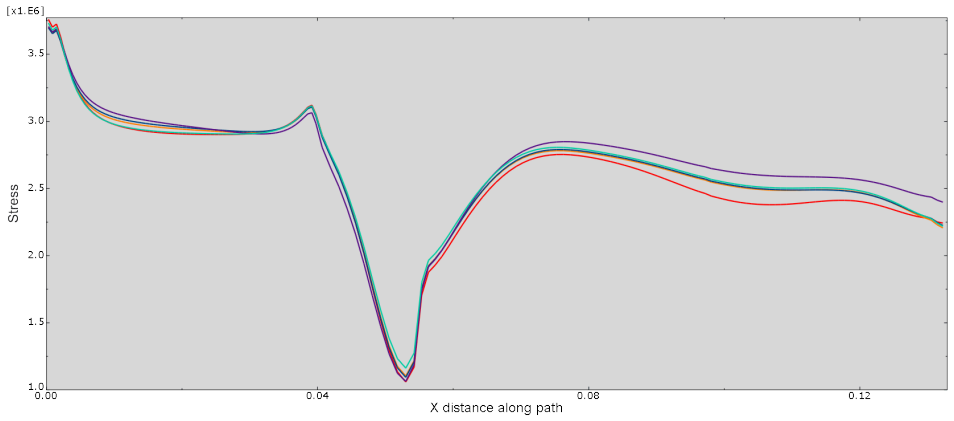


(c) Middle of ply-6

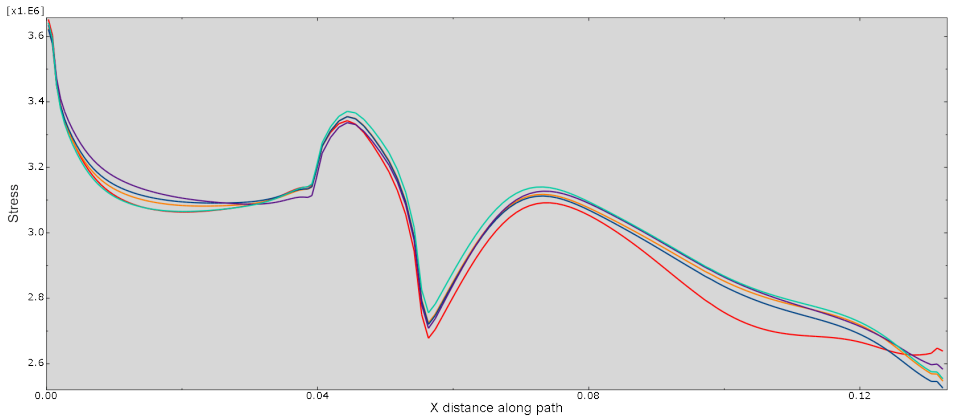


(d) Top of ply-15

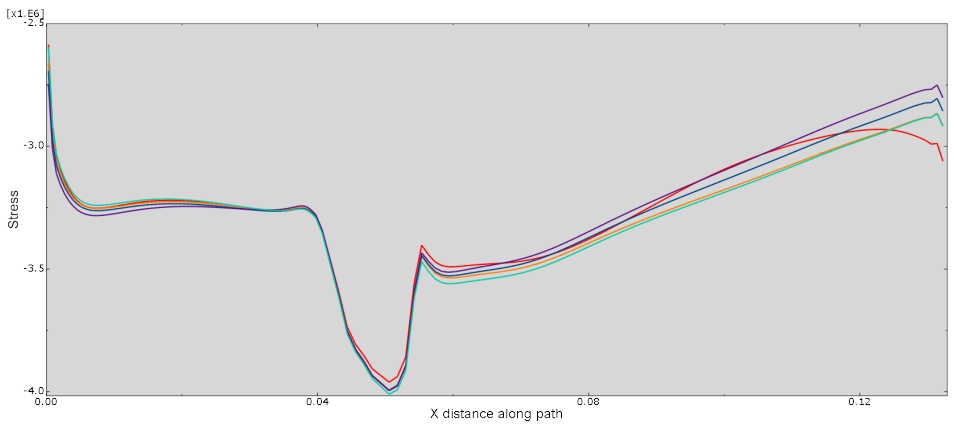
Figure 34: S12 submodel stresses at different plies of the outer skin. The ply is indicated in the caption of each subfigure. Stresses are in Pa, distances in m.



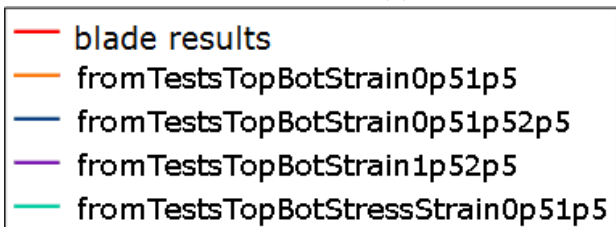
(a) Bottom of ply-1



(b) Top of ply-5



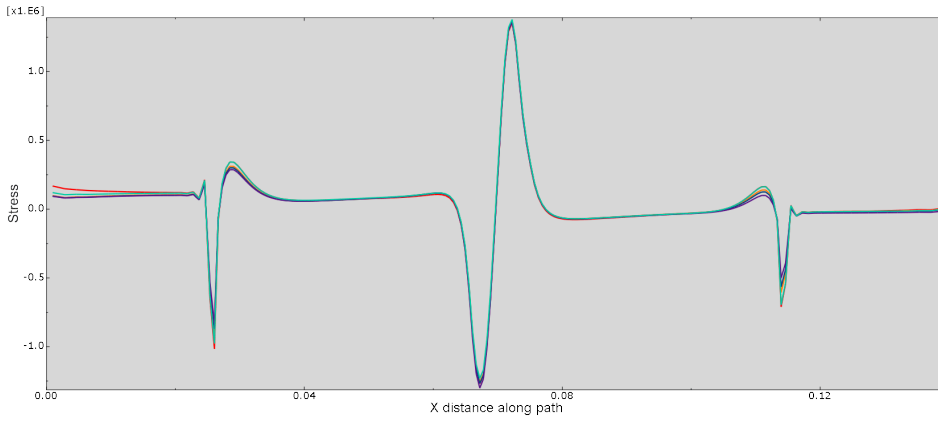
(c) Top of ply-10



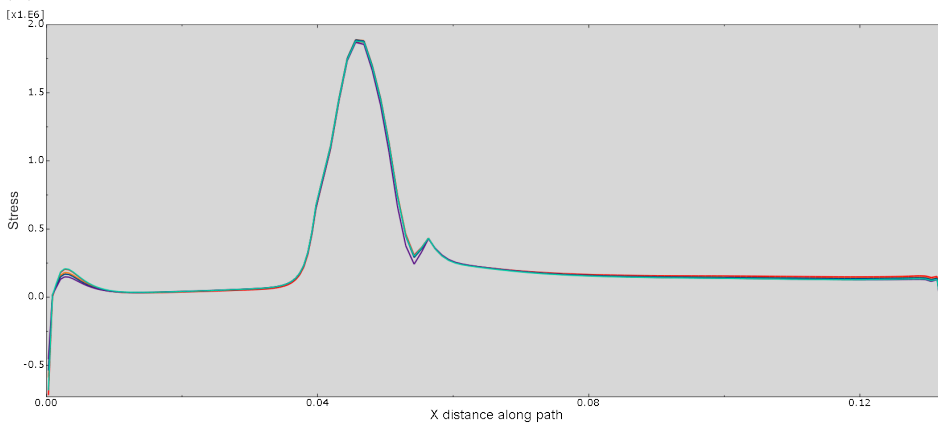
(d) legend

Figure 35: S12 submodel stresses at different plies of the shear web. The ply is indicated in the caption of each subfigure. Stresses are in Pa, distances in m.

Results for the through thickness stresses (S33) are provided below



(a) S33 submodel stresses next to the glue on the outer skin side of the glue



(b) S33 submodel stresses next to the glue on the shear web side of the glue. Stresses are in Pa, distances in m.

Figure 36: Through thickness stress in the submodel

5 Conclusions

The proposed method seems to lead to good results in the vicinity of the T-joint where the data to compare shell results has been extracted. The agreement for the through thickness stress is particularly good. These stresses are very relevant in the failure mechanism of T-joints under pull-out test loading [7]. The next steps to develop further the method could consider including the effect of the angle between the shear web and the outer skin, as this angle is not always 90 degrees in a real blade. This could be performed by having the same test cases with several angles, and then automatically identifying the angle in the blade from the mesh. The other topic that is of interest is the stiffness reduction of the joint as it gets damaged. A connector could be included in the blade shell model, joining the outer skin and the shear web, that would model the damage. Research could be carried out on how to determine the properties of the connectors to be used, so as to include a measure of the damage, and the right stiffness properties of the T-joint with damage. The damage in the T-joint to be modelled by a connector could encompass both the stiffness reduction with fatigue life in the composite itself, and also the fracture next to the glue reported in [7].

References

- [1] C. Bak et al. “Design and performance of a 10MW wind turbine”. In: *Danish Wind Power Research* (2013).

- [2] T. Burton et al. *Wind Energy Handbook*. Wiley, 2001.
- [3] J. Degrieck and W. Van Paepegem. “Fatigue damage modelling of fibre-reinforced composite materials: review”. In: *Applied Mechanics Reviews* 54.4 (2001), pp. 279–300.
- [4] H. Gulasik and D. Coker. “Delamination-debond behaviour of composite T-joints in wind turbine blades”. In: *The science of making torque from wind 2014, Journal of Physics Conference Series* 524.012043 (2014).
- [5] Amirhossein Hajdaei. “Extending the fatigue life of a T-joint in a composite wind turbine blade”. PhD thesis. Manchester University, 2013.
- [6] B. Pascual. *EP/L014106/1, Deliverable 5.1.1: Report on Stress concentration estimation method for innovative blade design*. Tech. rep. Supergen Wind Hub- Sustainable Power Generation and Supply-Wind Energy Technologies, 2017.
- [7] Y.Wang et al. “Finite element analysis of composite T-joints used in wind turbine blades”. In: *Plastics, Rubber and Composites* 44.3 (2016), pp. 87–97.